

Two-body wave functions and compositeness from scattering amplitudes: II. Application to the physical N^* and Δ^* resonances

Takayasu Sekihara^{1,2,3,*}

¹*Graduate School of Life and Environmental Science,*

Kyoto Prefectural University, Sakyo-ku, Kyoto 606-8522, Japan

²*Research Center for Nuclear Physics (RCNP), Osaka University, Ibaraki, Osaka, 567-0047, Japan*

³*RIKEN Cluster for Pioneering Research, RIKEN, Wako 351-0198, Japan*

(Dated: September 7, 2021)

The meson–baryon molecular components for the N^* and Δ^* resonances are investigated in terms of the compositeness, which is defined as the norm of the two-body wave function from the meson–baryon scattering amplitudes. The scattering amplitudes are constructed in a πN – ηN – σN – ρN – $\pi\Delta$ coupled-channels problem in a meson exchange model together with several bare N^* and Δ^* states, and parameters are fitted so as to reproduce the on-shell πN partial wave amplitudes up to the center-of-mass energy 1.9 GeV with the orbital angular momentum $L \leq 2$. As a result, the Roper resonance $N(1440)$ is found to be dominated by the πN and σN molecular components while the bare-state contribution is small. The squared wave functions in coordinate space imply that both in the πN and σN channels the separation between the meson and baryon is about more than 1 fm for the $N(1440)$ resonance. On the other hand, dominant meson–baryon molecular components are not observed in any other N^* and Δ^* resonances in the present model, although they have some fractions of the meson–baryon clouds.

I. INTRODUCTION

The spectroscopy of the nucleon resonances N^* and Δ^* is a key clue to understand nonperturbative aspects of quantum chromodynamics (QCD), which is the fundamental theory of hadrons and strong interactions [1]. Historically, the $\Delta(1232)$ resonance opens the door to the color degrees of freedom [2], which is an essential idea of QCD. The masses, widths, and other properties such as transition strength of the nucleon resonances have been good tests to examine the behavior of constituent quarks inside them. Today rich spectra of the nucleon resonances have been revealed in the πN coupled-channels scattering amplitudes by dynamical coupled-channels models [3–6] as well as the K -matrix approaches [7, 8]. In addition, results from the lattice QCD simulations have been used to discuss the N^* and Δ^* physics [9–13]. Recent studies on the N^* and Δ^* spectroscopy can be found in, e.g., Refs. [14–22]. Motivated by these rich spectra of the nucleon resonances, we are now in a phase of clarifying their internal structure.

In this study I utilize the πN scattering amplitudes for the calculations of the meson–baryon molecular components for the N^* and Δ^* resonances. This can be done in a strategy developed in my first paper of a series [23], where I have shown that the two-body wave function of the bound state, both in the stable and decaying cases, can be extracted from the residue of the off-shell scattering amplitude at the bound-state pole. Furthermore, the normalization of the two-body wave function from the residue is automatically achieved. In this sense, once the πN coupled-channels interactions are fixed so as to

reproduce the empirical πN scattering amplitudes, one can discuss the internal structure of the N^* and Δ^* resonances with the meson–baryon wave functions from the off-shell parts of the scattering amplitudes and its norm, which is called compositeness [24–27]. (For calculations of the compositeness, see, e.g., Refs. [28–41]. See also review articles on hadronic molecules [42] and hadron–hadron scattering [43].) In particular, from the πN scattering amplitudes I can unveil amounts of the meson–baryon molecular components of N^* and Δ^* resonances which are claimed to be “dynamically generated” without bare N^* and Δ^* states. Furthermore, even for the resonances which originate from bare states, I can evaluate how much the bare states are dressed in the meson–baryon clouds in terms of the compositeness. These are the aim of the present paper, the second paper of a series for the two-body wave function and compositeness in general quantum systems following the first paper [23].

This paper is organized as follows. First, I briefly show the formulae of the two-body wave function and compositeness from the scattering amplitude of constituents in Sec. II. Next, in Sec. III I construct an effective model to describe the πN scattering amplitudes and N^* and Δ^* resonances. In Sec. IV I utilize the πN scattering amplitudes in the effective model for the calculations of the two-body wave functions and compositeness for the N^* and Δ^* resonances, and I discuss their meson–baryon molecular components. Section V is devoted to the conclusion of this study.

II. FORMULAE OF COMPOSITENESS

First of all, I briefly summarize the formulae of the two-body wave functions and compositeness from the scattering amplitudes, which were expressed in detail in

*Electronic address: sekihara@post.j-parc.jp

Refs. [23, 31]. Below I focus on unstable resonance states, but formulations and equations are applicable to stable bound states as well. After showing general formulae in Sec. II A, I rewrite them in terms of the complex scaling method for numerical calculations of resonance wave functions in Sec. II B.

A. Two-body wave functions from scattering amplitudes

In this study I consider a two-body to two-body scattering, $k(\mathbf{q}) \rightarrow j(\mathbf{q}')$, where $k(\mathbf{q})$ and $j(\mathbf{q}')$ denote the channels (relative three-momenta) of the two-body initial and final states, respectively. The scattering is governed by the two-body interaction $V_{\alpha,jk}(E; q', q)$ in momentum space, where E is the center-of-mass energy of the system, $q^{(l)} \equiv |\mathbf{q}^{(l)}|$, and partial-wave projection to a certain quantum number α of the system was performed. I allow that the interaction may intrinsically depend on the energy E . Then, the scattering amplitude $T_{\alpha,jk}(E; q', q)$ in a coupled-channels problem is a solution of the Lippmann–Schwinger equation:

$$T_{\alpha,jk}(E; q', q) = V_{\alpha,jk}(E; q', q) + \sum_{l=1}^{N_{\text{chan}}} \int_0^\infty dk k^2 \frac{V_{\alpha,jl}(E; q', k) T_{\alpha,lk}(E; k, q)}{E - \mathcal{E}_l(k) + i0}. \quad (1)$$

Here N_{chan} is the number of channels and $\mathcal{E}_j(q)$ is the on-shell energy of the system in the j th channel as a function of the relative three-momentum q , for which I take the semirelativistic option:

$$\mathcal{E}_j(q) = \sqrt{m_j + q^2} + \sqrt{M_j + q^2}, \quad (2)$$

for stable particle channels, and

$$\mathcal{E}_j(E; q) = \sqrt{m_j + q^2} + \sqrt{M_j + q^2} + \Sigma_j(E; q), \quad (3)$$

for unstable particle channels with the self-energy Σ_j whose practical form is given in Sec. III C. The masses of two particles in the j th channel are m_j and M_j .

In my model space I treat only two-body to two-body scattering. In the study of the N^* and Δ^* resonances below, I will implement one-body states (bare N^* and Δ^*) into the two-body interaction $V_{\alpha,jk}$ and three-body state ($\pi\pi N$) into the self-energy Σ_j .

In the physical scattering, the initial and final states are on their mass shell, $E = \mathcal{E}_j(q') = \mathcal{E}_k(q)$, and hence the scattering amplitude $T_{\alpha,jk}(E; q', q)$ is a function only of the energy E , which is called the on-shell amplitude. The on-shell amplitude is a solution of the Lippmann–Schwinger equation (1) and can be evaluated by the Heitler equation

$$T_{\alpha,jk}^{\text{on-shell}}(E) = K_{\alpha,jk}^{\text{on-shell}}(E) + \sum_{l=\text{stable}} K_{\alpha,jl}^{\text{on-shell}}(E) \left[-i \frac{\rho_l(E)}{2} \right] T_{\alpha,lk}^{\text{on-shell}}(E), \quad (4)$$

with the on-shell K -matrix $K_{\alpha,jk}^{\text{on-shell}}$ and phase space ρ_l where l represents channels of stable particles. The K -matrix is a solution of the following equation

$$K_{\alpha,jk}(E; q', q) = V_{\alpha,jk}(E; q', q) + \sum_{l=1}^{N_{\text{chan}}} \mathcal{P} \int_0^\infty dk k^2 \frac{V_{\alpha,jl}(E; q', k) K_{\alpha,lk}(E; k, q)}{E - \mathcal{E}_l(k)}, \quad (5)$$

and its on-shell part, $K_{\alpha,jk}^{\text{on-shell}}$, is obtained by taking the on-shell momenta q' and q for the parameters of $K_{\alpha,jk}$ as $\mathcal{E}_j(q') = \mathcal{E}_k(q) = E$. By means of \mathcal{P} I take the Cauchy principal value for the integral over the momentum variable in stable open channels, but it returns to the usual integral in closed channels or unstable channels. The phase space is defined for stable channels as

$$\rho_j(E) = \frac{E^4 - (m_j^2 - M_j^2)^2}{4\pi E^3} k_j(E) \theta(E - m_j - M_j), \quad (6)$$

with the Heaviside step function $\theta(x)$ and the on-shell relative three-momentum

$$k_j(E) = \frac{\lambda^{1/2}(E^2, m_j^2, M_j^2)}{2E}. \quad (7)$$

Here $\lambda(x, y, z) \equiv x^2 + y^2 + z^2 - 2xy - 2yz - 2zx$ is the Källén function.

Besides the on-shell amplitude, mathematically one may treat $T_{\alpha,jk}(E; q', q)$ as a function of the three independent variables E , q' , and q as an off-shell amplitude. In particular, calculation of the off-shell amplitude with the complex energy E is essential to extract the two-body wave function from the scattering amplitude, as seen below.

The scattering amplitude may have resonance poles in the complex energy plane. Each pole position E_{pole} coincides with an eigenvalue of the Schrödinger equation for a resonance state as an eigenstate. The pole for a certain resonance state exists at the same position in the on-shell and off-shell amplitudes. In particular, the resonance pole in the off-shell amplitude can be described as

$$T_{\alpha,jk}(E; q', q) = \frac{\gamma_j(q') \gamma_k(q)}{E - E_{\text{pole}}} + (\text{regular at } E = E_{\text{pole}}), \quad (8)$$

with the residue $\gamma_j(q') \gamma_k(q)$.

As pointed out first by Weinberg [44] and discussed in Refs. [23, 31], the residue of the off-shell amplitude contains information on the two-body wave function of the corresponding resonance state as

$$\gamma_j(q) = \frac{1}{(2\pi)^{3/2}} [E_{\text{pole}} - \mathcal{E}_j(q)] \tilde{R}_j(q), \quad (9)$$

where $\tilde{R}_j(q)$ is the radial part of the resonance wave function in the j th channel in momentum space. An important point is that one cannot introduce any scaling factor for this wave function $\tilde{R}_j(q)$ because the Lippmann–Schwinger equation (1) is an inhomogeneous integral

equation. Therefore, the wave function in Eq. (9) should be automatically scaled. Indeed, the normalization of the wave function in Eq. (9) is guaranteed by the fact that the residue of the resonance propagator $1/(E-\hat{H})$, where \hat{H} is the full Hamiltonian, is chosen to be exactly unity in the present formulation [23].

From the residue, one can calculate the norm of the two-body wave function in the j th channel. In the present notation, the expression of the norm is

$$X_j = \int_0^\infty dq \tilde{P}_j(q), \quad (10)$$

with the density distribution $\tilde{P}_j(q)$ defined as

$$\tilde{P}_j(q) \equiv \frac{q^2}{(2\pi)^3} \tilde{R}_j(q)^2 = q^2 \left[\frac{\gamma_j(q)}{E_{\text{pole}} - \mathcal{E}_j(q)} \right]^2. \quad (11)$$

I call X_j the compositeness of the channel j for the resonance state. Here I note that in Eq. (11) one should calculate the complex number squared rather than the absolute value squared so as to achieve the normalizability for resonance wave functions [45].

The wave function in coordinate space can be calculated by the Fourier transformation, which brings the radial part of the wave function in coordinate space $R_j(r)$:

$$R_j(r) = \frac{i^L}{2\pi^2} \int_0^\infty dq q^2 \tilde{R}_j(q) j_L(qr), \quad (12)$$

where $j_L(x)$ is the spherical Bessel function with the orbital angular momentum L for the channel j . Therefore, after omitting the irrelevant factor i^L from the angular part, the density distribution in coordinate space becomes

$$\begin{aligned} P_j(r) &= r^2 \left[\frac{1}{2\pi^2} \int_0^\infty dq q^2 \tilde{R}_j(q) j_L(qr) \right]^2 \\ &= \frac{2r^2}{\pi} \left[\int_0^\infty dq q^2 \frac{\gamma_j(q)}{E_{\text{pole}} - \mathcal{E}_j(q)} j_L(qr) \right]^2, \end{aligned} \quad (13)$$

which is related to the compositeness as

$$X_j = \int_0^\infty dr P_j(r). \quad (14)$$

Because the wave function from the scattering amplitude is automatically scaled, the compositeness (10) and (14) should be normalized correctly. Indeed, for energy-independent interactions, the compositeness was proved to be exactly unity in Ref. [45] in the nonrelativistic single-channel resonances, and the validity was extended to coupled-channels problems in semirelativistic cases in Ref. [23].

However, when one treats energy dependent interaction and/or unstable constituent with its self-energy, the sum of the compositeness of all channels deviates from unity. This can be interpreted as a missing-channel contribution, which is not explicit degrees of freedom in the

model space of the two-body channels but is implemented into the interaction and/or into the self-energy. I represent the missing-channel contribution as Z :

$$Z \equiv 1 - \sum_{j=1}^{N_{\text{chan}}} X_j. \quad (15)$$

Here I note that both the compositeness X_j and the missing-channel contribution Z are model dependent quantities because they are not physical observables (see discussion in Ref. [23]).

For resonance states, the compositeness X_j and the missing-channel contribution Z become complex in general. Therefore, in contrast to the stable bound states, one cannot make a probabilistic interpretation for them. Actually, for stable bound states, X_j and Z are real and bound in the range $[0, 1]$ and hence a sum rule

$$\sum_{j=1}^{N_{\text{chan}}} |X_j| + |Z| = 1 \quad (16)$$

is satisfied. On the other hand, this relation is not satisfied for resonance states because both X_j and Z are complex. To interpret such complex values, I introduce a quantity U for resonance states to measure the deviation from the sum rule (16), according to Refs. [30, 37]

$$U \equiv \sum_{j=1}^{N_{\text{chan}}} |X_j| + |Z| - 1. \quad (17)$$

Because of the definition of Z in Eq. (15), U satisfies $U \geq 0$. Furthermore, U becomes small if $\text{Im} X_j$ and $\text{Im} Z$ are negligible and $\text{Re} X_j$ and $\text{Re} Z$ are not negatively large. In such a case, the wave function of the resonance state considered is similar to that of a certain stable bound state. In particular, U goes to zero in a stable bound-state limit, so U is understood as an uncertainty of the interpretation of the complex-valued X_j and Z , as discussed in Refs [30, 37].

In this line, I employ quantities introduced in Refs. [23, 31]:

$$\tilde{X}_j \equiv \frac{|X_j|}{1+U}, \quad \tilde{Z} \equiv \frac{|Z|}{1+U}. \quad (18)$$

The quantities \tilde{X}_j and \tilde{Z} are real, bound in the range $[0, 1]$, and automatically satisfy the sum rule:

$$\sum_{j=1}^{N_{\text{chan}}} \tilde{X}_j + \tilde{Z} = 1. \quad (19)$$

Then, to estimate uncertainties of the probabilistic interpretation of \tilde{X}_j and \tilde{Z} , I utilize the relation (17), which means that U measures the deviation from sum rule for a bound state (16). Therefore, a contribution from each

X_j or Z to the deviation U can be estimated by U divided by the number of the degrees of freedom $N_{\text{chan}} + 1$, to which I refer as the reduced uncertainty U_r :

$$U_r \equiv \frac{U}{N_{\text{chan}} + 1}. \quad (20)$$

In this sense, if and only if $U_r \ll 1$, one can interpret \tilde{X}_j (\tilde{Z}) as the probability of finding the composite (missing) part, and U_r can be considered as the uncertainty of the probabilities \tilde{X}_j and \tilde{Z} .

B. Complex scaling method for resonances

To calculate numerically the resonance wave function from the residue of the scattering amplitude, one has to perform an analytic continuation to reach the resonance pole E_{pole} in the complex energy plane. One way to do this is the complex scaling method [46, 47], which I employ in the present study.

In the complex scaling method, one transforms the relative coordinate \mathbf{r} and relative momenta \mathbf{q} for two-body states into the complex-scaled values in the following manner:

$$\mathbf{r} \rightarrow \mathbf{r}e^{i\theta}, \quad \mathbf{q} \rightarrow \mathbf{q}e^{-i\theta}, \quad (21)$$

with the scaling angle θ . Then, the equations relevant to my study become:

$$\begin{aligned} T_{\alpha,jk}(E; q'e^{-i\theta}, qe^{-i\theta}) &= V_{\alpha,jk}(E; q'e^{-i\theta}, qe^{-i\theta}) \\ &+ e^{-3i\theta} \sum_{l=1}^{N_{\text{chan}}} \int_0^\infty dk k^2 \frac{V_{\alpha,jl}(E; q'e^{-i\theta}, ke^{-i\theta})}{E - \mathcal{E}_l(ke^{-i\theta})} \\ &\times T_{\alpha,lk}(E; ke^{-i\theta}, qe^{-i\theta}), \end{aligned} \quad (22)$$

$$\begin{aligned} T_{\alpha,jk}(E; q'e^{-i\theta}, qe^{-i\theta}) \\ = \frac{\gamma_j(q'e^{-i\theta})\gamma_k(qe^{-i\theta})}{E - E_{\text{pole}}} + (\text{regular at } E = E_{\text{pole}}), \end{aligned} \quad (23)$$

$$\gamma_j(qe^{-i\theta}) = \frac{1}{(2\pi)^{3/2}} [E_{\text{pole}} - \mathcal{E}_j(qe^{-i\theta})] \tilde{R}_j(qe^{-i\theta}), \quad (24)$$

$$X_j = \int_0^\infty dq \tilde{P}_j^{(\theta)}(q) = \int_0^\infty dr P_j^{(\theta)}(r), \quad (25)$$

$$\tilde{P}_j^{(\theta)}(q) = e^{-3i\theta} q^2 \left[\frac{\gamma_j(qe^{-i\theta})}{E_{\text{pole}} - \mathcal{E}_j(qe^{-i\theta})} \right]^2, \quad (26)$$

$$P_j^{(\theta)}(r) = \frac{2r^2 e^{-3i\theta}}{\pi} \left[\int_0^\infty dq q^2 \frac{\gamma_j(qe^{-i\theta}) j_L(qr)}{E_{\text{pole}} - \mathcal{E}_j(qe^{-i\theta})} \right]^2. \quad (27)$$

The definitions of the missing-channel contribution Z (15), uncertainties U (17) and U_r (20), and real-valued quantities \tilde{X} and \tilde{Z} (18) are unchanged.

An important property of the complex scaling method is that the pole position E_{pole} and compositeness X_j do not depend on the scaling angle θ while density distributions $P_j^{(\theta)}$ and $\tilde{P}_j^{(\theta)}$ depend on θ .

III. THE πN COUPLED-CHANNELS SCATTERING AMPLITUDES

As described in the previous section, one can extract normalized two-body wave functions of resonance states from the residues of the off-shell scattering amplitudes at the resonance poles. This fact is of special important when investigating the internal structure of the N^* and Δ^* resonances, because nowadays precise πN scattering amplitudes are available from the partial wave analysis of the experimental data (see, e.g., the database of SAID [48]), which allows us to construct sophisticated models for the πN coupled-channels scattering amplitudes as done in Refs. [5, 6].

In this study I investigate the meson–baryon molecular components of the N^* and Δ^* resonances by constructing a meson–baryon coupled-channels model for the πN amplitudes partly based on Ref. [49]. For this purpose I take into account the πN , ηN , σN , ρN , and $\pi\Delta$ channels. The interactions are calculated according to the Feynman diagrams shown in Fig. 1. Model parameters are fixed so as to reproduce the results of the SAID partial wave analysis for the on-shell πN amplitudes [48] up to $E = 1.9$ GeV with the orbital angular momentum $L \leq 2$, i.e., S_{11} , S_{31} , P_{11} , P_{31} , P_{13} , P_{33} , D_{13} , D_{33} , D_{15} , and D_{35} partial waves of the elastic πN scattering. Here and below I use the notation L_{2I2J} with the orbital angular momentum L , isospin I , and total angular momentum J for the πN system.

I first summarize the notation of the πN scattering amplitudes in Sec. III A and then construct the tree-level interactions in Sec. III B. The self-energies for the unstable channels, i.e., σN , ρN , and $\pi\Delta$, are introduced in Sec. III C. In Sec. III D bare N^* and Δ^* states are introduced. Finally in Sec. III E the model parameters are fitted to reproduce the on-shell πN partial wave amplitudes. Throughout the calculations isospin symmetry is assumed.

A. Notation of the scattering amplitudes

First of all, I fix the quantum number of the πN scattering. When one considers the elastic πN scattering, its partial wave can be uniquely specified by L_{2I2J} . In a general coupled-channels analysis, however, the quantum number of the system should be specified by the spin/parity J^P and isospin I , because the orbital angular momentum L may change in different channels such as

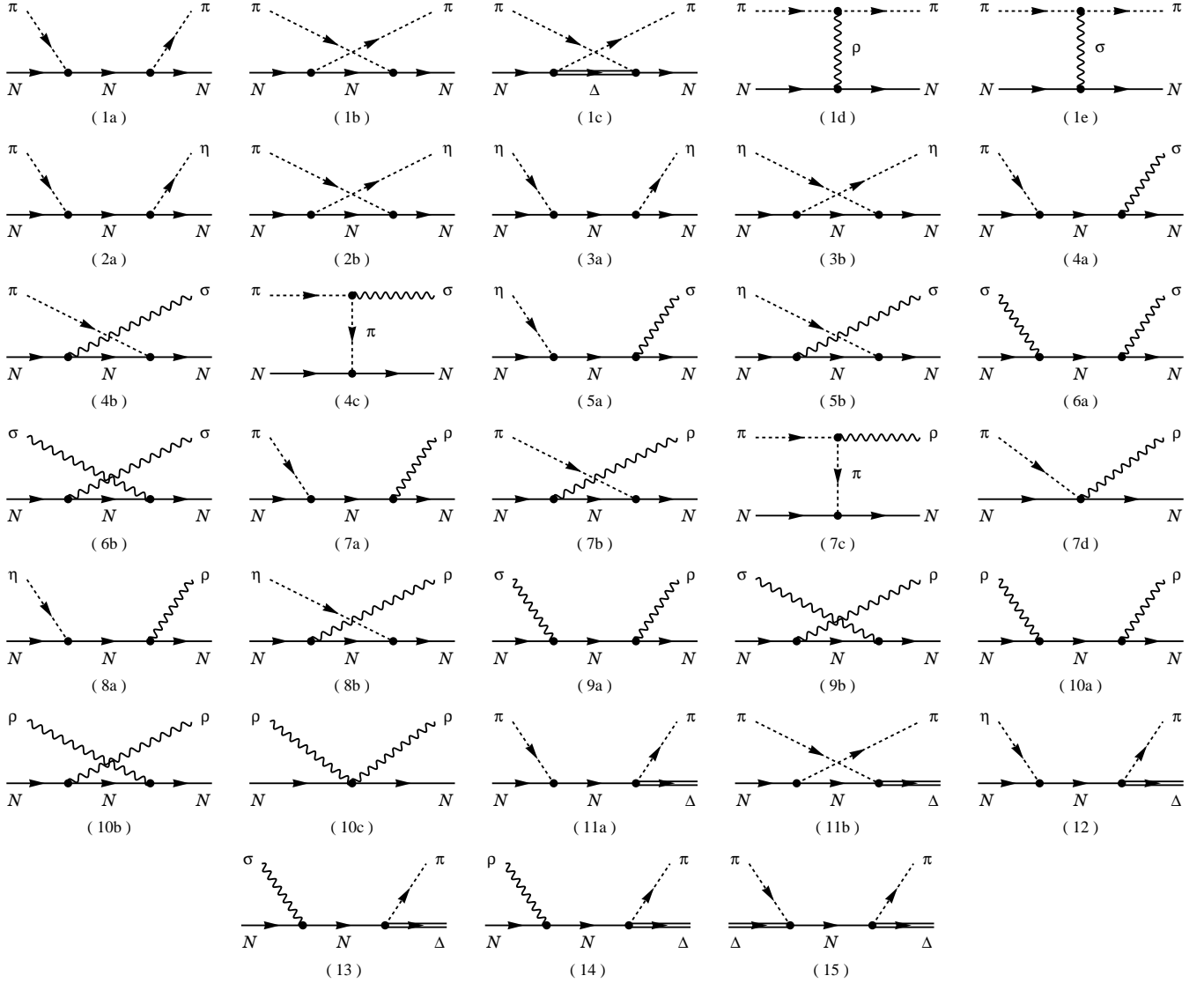


FIG. 1: Feynman diagrams for the meson–baryon interactions in the πN coupled-channels scattering amplitudes.

TABLE I: Explicit channels for each quantum number J^P, I ($L_{2I}2J$ for the elastic πN) considered in the present study. The meson–baryon states are specified by their orbital angular momentum L and total spin S as (L, S) .

$J^P, I (L_{2I}2J)$	Channel 1	Channel 2	Channel 3	Channel 4	Channel 5	Channel 6	Channel 7	Channel 8
$1/2^-, 1/2 (S_{11})$	$\pi N(0, 1/2)$	$\eta N(0, 1/2)$	$\sigma N(1, 1/2)$	$\rho N(0, 1/2)$	$\rho N(2, 3/2)$	$\pi \Delta(2, 3/2)$		
$1/2^-, 3/2 (S_{31})$	$\pi N(0, 1/2)$	$\rho N(0, 1/2)$	$\rho N(2, 3/2)$	$\pi \Delta(2, 3/2)$				
$1/2^+, 1/2 (P_{11})$	$\pi N(1, 1/2)$	$\eta N(1, 1/2)$	$\sigma N(0, 1/2)$	$\rho N(1, 1/2)$	$\rho N(1, 3/2)$	$\pi \Delta(1, 3/2)$		
$1/2^+, 3/2 (P_{31})$	$\pi N(1, 1/2)$	$\rho N(1, 1/2)$	$\rho N(1, 3/2)$	$\pi \Delta(1, 3/2)$				
$3/2^+, 1/2 (P_{13})$	$\pi N(1, 1/2)$	$\eta N(1, 1/2)$	$\sigma N(2, 1/2)$	$\rho N(1, 1/2)$	$\rho N(1, 3/2)$	$\pi \Delta(1, 3/2)$		
$3/2^+, 3/2 (P_{33})$	$\pi N(1, 1/2)$	$\rho N(1, 1/2)$	$\rho N(1, 3/2)$	$\pi \Delta(1, 3/2)$				
$3/2^-, 1/2 (D_{13})$	$\pi N(2, 1/2)$	$\eta N(2, 1/2)$	$\sigma N(1, 1/2)$	$\rho N(0, 3/2)$	$\rho N(2, 1/2)$	$\rho N(2, 3/2)$	$\pi \Delta(0, 3/2)$	$\pi \Delta(2, 3/2)$
$3/2^-, 3/2 (D_{33})$	$\pi N(2, 1/2)$	$\rho N(0, 3/2)$	$\rho N(2, 1/2)$	$\rho N(2, 3/2)$	$\pi \Delta(0, 3/2)$	$\pi \Delta(2, 3/2)$		
$5/2^-, 1/2 (D_{15})$	$\pi N(2, 1/2)$	$\eta N(2, 1/2)$	$\rho N(2, 1/2)$	$\rho N(2, 3/2)$	$\pi \Delta(2, 3/2)$			
$5/2^-, 3/2 (D_{35})$	$\pi N(2, 1/2)$	$\rho N(2, 1/2)$	$\rho N(2, 3/2)$	$\pi \Delta(2, 3/2)$				

TABLE II: Effective Lagrangians for the πN coupled-channels interaction.

Vertex	\mathcal{L}_{int}
πNN	$-\frac{D+F}{2f_\pi} \bar{N} \gamma^\mu \gamma_5 \partial_\mu \vec{\pi} \cdot \vec{\tau} N$
$\pi N \Delta$	$-\frac{f_{\pi N \Delta}}{m_\pi} \bar{N} \partial_\mu \vec{\pi} \cdot \vec{T} \Delta^\mu + \text{h.c.}$
ρNN	$\frac{g_{\rho NN}}{2} \bar{N} \left(\gamma^\mu - \frac{\kappa_\rho}{2m_N} \sigma^{\mu\nu} \partial_\nu \right) \vec{\rho}_\mu \cdot \vec{\tau} N$
$\pi \pi \rho$	$g_{\pi \pi \rho} (\vec{\pi} \times \partial^\mu \vec{\pi}) \cdot \vec{\rho}_\mu$
σNN	$g_{\sigma NN} \sigma \bar{N} N$
$\pi \pi \sigma$	$-\frac{g_{\pi \pi \sigma}}{2m_\pi} \partial_\mu \vec{\pi} \cdot \partial^\mu \vec{\pi} \sigma$
ηNN	$\frac{D-3F}{2\sqrt{3}f_\eta} \partial_\mu \eta \bar{N} \gamma^\mu \gamma_5 N$
$\pi \rho NN$	$\frac{(D+F)g_{\rho NN}}{2f_\pi} \bar{N} \gamma^\mu \gamma_5 (\vec{\pi} \times \vec{\rho}_\mu) \cdot \vec{\tau} N$
$\rho \rho NN$	$\frac{g_{\rho NN}^2 \kappa_\rho}{8m_N} \bar{N} \sigma^{\mu\nu} (\vec{\rho}_\mu \times \vec{\rho}_\nu) \cdot \vec{\tau} N$

πN and σN . Therefore, for the coupled-channels scattering amplitude in the Lippmann–Schwinger equation (1), I use the notation $\alpha = (J^P, I)$, but for the πN partial waves I use the notation $L_{2I 2J}$ as well.

For each quantum number $\alpha = (J^P, I)$, I take into account the πN , ηN , σN , ρN , and $\pi \Delta$ channels with their orbital angular momenta $L \leq 2$. The explicit channels considered are summarized in Table I. From the coupled-channels amplitude, I calculate the normalized on-shell πN amplitude $L_{2I 2J}(E)$ as

$$L_{2I 2J}(E) = -\frac{\rho_{\pi N}(E)}{2} T_{(J^P, I), 11}^{\text{on-shell}}(E), \quad (28)$$

where the phase space $\rho_{\pi N}$ of the πN channel is calculated according to Eq. (6). This normalized πN amplitude satisfies the optical theorem

$$\text{Im} L_{2I 2J}(E) = |L_{2I 2J}(E)|^2. \quad (29)$$

below the inelastic threshold for the πN state.

B. Tree-level interactions

Next I formulate the tree-level πN coupled-channels interactions diagrammatically shown in Fig. 1. For this purpose I employ effective Lagrangians summarized in Table II. Here the notations for the hadron fields are: $N = (p, n)^t$ and

$$\vec{\pi} = (\pi^1, \pi^2, \pi^3) = \left(\frac{\pi^+ + \pi^-}{\sqrt{2}}, -\frac{\pi^+ - \pi^-}{\sqrt{2}i}, \pi^0 \right), \quad (30)$$

hence

$$\vec{\pi} \cdot \vec{\tau} = \begin{pmatrix} \pi^0 & \sqrt{2}\pi^+ \\ \sqrt{2}\pi^- & -\pi^0 \end{pmatrix}, \quad (31)$$

where $\vec{\tau} = (\tau^1, \tau^2, \tau^3)$ is the Pauli matrices acting on the isospin states. The $\vec{\rho}$ field is expressed in the same manner to the $\vec{\pi}$ field. The Δ field $\Delta = (\Delta^{++}, \Delta^+, \Delta^0, \Delta^-)^t$ is tied to the isospin transition operators $\vec{T} = (T^1, T^2, T^3)$ from isospin 3/2 to 1/2:

$$T^1 = \begin{pmatrix} -1/\sqrt{2} & 0 & 1/\sqrt{6} & 0 \\ 0 & -1/\sqrt{6} & 0 & 1/\sqrt{2} \end{pmatrix}, \quad (32)$$

$$T^2 = \begin{pmatrix} -i/\sqrt{2} & 0 & -i/\sqrt{6} & 0 \\ 0 & -i/\sqrt{6} & 0 & -i/\sqrt{2} \end{pmatrix}, \quad (33)$$

$$T^3 = \begin{pmatrix} 0 & \sqrt{2/3} & 0 & 0 \\ 0 & 0 & \sqrt{2/3} & 0 \end{pmatrix}, \quad (34)$$

hence

$$\vec{\pi} \cdot \vec{T} = \begin{pmatrix} -\pi^- & \sqrt{2/3}\pi^0 & \sqrt{1/3}\pi^+ & 0 \\ 0 & -\sqrt{1/3}\pi^- & \sqrt{2/3}\pi^0 & \pi^+ \end{pmatrix}. \quad (35)$$

For the πNN and ηNN vertices, I employ the chiral Lagrangian with the meson decay constants, f_π and f_η , at their physical values [1], $f_\pi = 92.1 \text{ MeV}$ and $f_\eta = 1.3f_\pi$, and fix the coupling constants $D + F = 1.26$ and $D - F = 0.33$ by the weak decay of octet baryons. Therefore, both the πNN and ηNN couplings do not contain free parameters, except for the cutoffs [see Eq. (36)].

As for the $\pi N \Delta$ vertex, I treat the coupling constant $f_{\pi N \Delta}$ as a free parameter. I use the real-valued physical $\Delta(1232)$ mass $m_\Delta = 1210 \text{ MeV}$ for the propagator of the diagram (1c) in Fig. 1. I allow that the parameters for the Δ in the diagram (1c) may differ from those for the bare Δ introduced in Sec. III D for better reproduction of the experimental data.

In the case of the ρ and σ exchanges, the coupling constants $g_{\rho NN}$, κ_ρ , $g_{\pi \pi \rho}$, $g_{\sigma NN}$, and $g_{\pi \pi \sigma}$ are free parameters. For these t -channel ρ and σ exchanges, I use the real-valued physical mass for the ρ meson, $m_\rho = 775.3 \text{ MeV}$, but a real-valued bare mass for the σ meson, $m_{\sigma_0} = 700 \text{ MeV}$ (see Sec. III C).

To regularize the divergences from the integrals of the Lippmann–Schwinger equation (1), I introduce a dipole form factor

$$\mathcal{F}(\Lambda, q) \equiv \left(\frac{\Lambda^2}{\Lambda^2 + q^2} \right)^2, \quad (36)$$

with a cutoff Λ for each meson–baryon–baryon vertex with q being the three-momentum of the meson. I also use the dipole form factor (36) for the meson–meson–meson vertex with q being the three-momentum of the exchanged meson. The cutoffs Λ are model parameters and may take different values for different vertices.

The energies of the mesons and baryons in the initial and final states are respectively fixed to their on-shell values [see Eq. (B2) in Appendix B]. Therefore, the meson–baryon interactions of the diagrams in Fig. 1 do not depend on the center-of-mass energy E but only on the relative momenta q and q' . The explicit forms of the interaction terms and their partial-wave projections are given in Appendix C.

C. Self-energies for the σN , ρN , and $\pi\Delta$ channels

Let us turn to the self-energies for the σN , ρN , and $\pi\Delta$ channels.

Because the σ , ρ , and Δ resonances are unstable particles, one should take into account their self-energies as in Eq. (3). I take the strategy to calculate the self-energy developed in Refs. [6, 50]. For the ρ and Δ resonances, I use the same formulae and parameters in Ref. [6]. On the other hand, to describe the σ resonance I use the same formula but different parameters so as to reproduce the $\pi\pi$ ($I = 0, L = 0$) phase shift in particular near the $\pi\pi$ threshold where the σ resonance exists. The effective interaction of the $\pi\pi$ ($I = 0, L = 0$) scattering is

$$\mathcal{V}_\sigma(E_2; q', q) = \frac{g_0}{E_2 - m_{\sigma_0}} f_g(q') f_g(q) + h_0 f_h(q') f_h(q), \quad (37)$$

with monopole form factors

$$f_g(q) = \frac{\lambda_g^2}{q^2 + \lambda_g^2}, \quad f_h(q) = \frac{\lambda_h^2}{q^2 + \lambda_h^2}. \quad (38)$$

Here E_2 is the total energy of the $\pi\pi$ system and $q^{(\prime)}$ is the relative momentum of the initial (final) $\pi\pi$ state. The bare σ mass m_{σ_0} , coupling constants g_0 and h_0 , and cutoffs λ_g and λ_h are the model parameters for the σ resonance. As a result of the fit to the $\pi\pi$ ($I = 0, L = 0$) phase shift, I obtain $m_{\sigma_0} = 700$ MeV, $g_0 = 616$ GeV $^{-1}$, $h_0 = 1189$ GeV $^{-2}$, $\lambda_g = 178$ MeV, and $\lambda_h = 217$ MeV for the σ resonance.

With the parameters for the σ , ρ , and Δ resonances, I find resonance poles at $E_2 = 486 - 213i$ MeV, $765 - 75i$ MeV, and $1210 - 55i$ MeV for the σ , ρ , and Δ resonances, respectively.

The σN , ρN , and $\pi\Delta$ self-energies, $\Sigma_{\sigma N}$, $\Sigma_{\rho N}$, and $\Sigma_{\pi\Delta}$, respectively, are calculated in the same manner as in Ref. [6], and then I obtain the kinetic energy (3) in these channels:

$$\mathcal{E}_{\sigma N}(E; q) = \sqrt{m_{\sigma_0}^2 + q^2} + \sqrt{m_N^2 + q^2} + \Sigma_{\sigma N}(E; q), \quad (39)$$

$$\mathcal{E}_{\rho N}(E; q) = \sqrt{m_{\rho_0}^2 + q^2} + \sqrt{m_N^2 + q^2} + \Sigma_{\rho N}(E; q), \quad (40)$$

$$\mathcal{E}_{\pi\Delta}(E; q) = \sqrt{m_\pi^2 + q^2} + \sqrt{m_{\Delta_0}^2 + q^2} + \Sigma_{\pi\Delta}(E; q), \quad (41)$$

with the bare ρ mass $m_{\rho_0} = 812$ MeV and bare Δ mass $m_{\Delta_0} = 1280$ MeV [6]. I note that the kinetic energies for the unstable channels as well as the self-energies depend on the energy E because they implicitly involve the three-body $\pi\pi N$ state. Therefore, this E dependence in the kinetic energy may give a deviation of the compositeness from unity and hence a nonzero missing-channel contribution Z (15) corresponding to the implicit $\pi\pi N$ state, as discussed in Ref. [23].

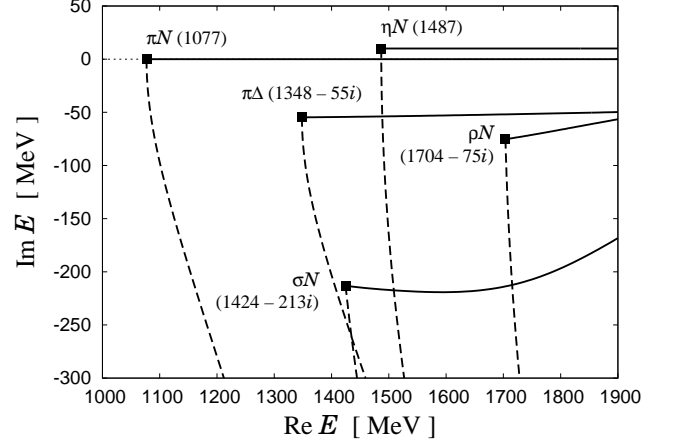


FIG. 2: Branch cuts for the πN , ηN , σN , ρN , and $\pi\Delta$ channels. The solid lines indicate the usual cuts, i.e., cuts with the complex-scaling angle $\theta = 0^\circ$, while the dashed lines are those with $\theta = 45^\circ$. The line for the ηN channel is shifted slightly upward for a better visualization. The boxes denote the branch points, whose positions are written in the parentheses in units of MeV.

By calculating the energy E which satisfies $E = \mathcal{E}_{\sigma N, \rho N, \pi\Delta}(E; q)$ with the momentum q from 0 to $+\infty$, I obtain the branch cuts for these channels, which are plotted in Fig. 2 as solid lines together with the branch cuts for the stable channels πN and ηN . I note that for the energy satisfying $\text{Re } E > 2m_\pi + m_N = 1215$ MeV and $\text{Im } E < 0$ I perform the analytic continuation to the second Riemann sheet of the $\pi\pi N$ channel by deforming appropriately the momentum integral paths in the formulae of the self-energies.

Here it is instructive to see how these branch cuts behave with a finite value of the complex-scaling angle θ in the complex scaling method. For this purpose, in Fig. 2 I also plot the branch cuts with $\theta = 45^\circ$ in the complex scaling method as the dashed lines. As one can see, each branch cut rotates clockwise with a finite value of the scaling angle. In practical calculations, one can reach the second Riemann sheet in each channel for the complex energy E in the region sandwiched between the solid and dashed lines of Fig. 2.

Finally I comment on the three-body unitarity. In the πN scattering the $\pi\pi N$ three-body channel opens at the $\pi\pi N$ threshold. In the present model I implicitly include the $\pi\pi N$ discontinuities arising from the s -channel propagation of the three-body states in the self-energies for the σN , ρN , and $\pi\Delta$ channels. The three-body cut for this process is depicted in Figs. 3(a) and 3(b) as the thick dashed lines. On the other hand, I do not include the $\pi\pi N$ discontinuities induced by the t -channel π exchanges in the $\pi\Delta \rightarrow \sigma N$, ρN transitions and by the u -channel N exchange in the $\pi\Delta \rightarrow \pi\Delta$ transition, which are depicted in Figs. 3(c) and 3(d), respectively. In this sense, I partly take into account the $\pi\pi N$ three-body unitarity. To satisfy the three-body $\pi\pi N$ unitarity fully, it

TABLE III: Bare N^* and Δ^* states introduced in the present model. Their fitted bare masses M_0 , cutoffs Λ , and coupling constants g are also shown. The channels are specified by the indices 1, 2, ..., 8 in the same order as in Table I.

$J^P, I (L_{2I} 2J)$	M_0 [MeV]	Λ [MeV]	g_1	g_2	g_3	g_4	g_5	g_6	g_7	g_8
$1/2^-, 1/2 (S_{11})$	1919	855	2.054	-0.570	0.415	-1.817	-0.031	-0.043		
"	2150	575	1.095	-0.761	-0.227	-2.651	-0.386	0.181		
$1/2^+, 1/2 (P_{11})$	1912	634	-1.116	0.299	2.221	0.157	0.719	0.610		
$3/2^+, 3/2 (P_{33})$	1314	476	1.089	-0.310	-0.288	0.046				
$3/2^-, 1/2 (D_{13})$	2043	608	0.148	0.033	-1.028	-1.935	-0.152	-0.213	-0.149	-0.068
$3/2^-, 3/2 (D_{33})$	1824	446	0.168	-2.488	0.142	0.262	2.762	0.150		
$5/2^-, 1/2 (D_{15})$	1821	494	0.142	0.189	0.060	0.096	0.167			

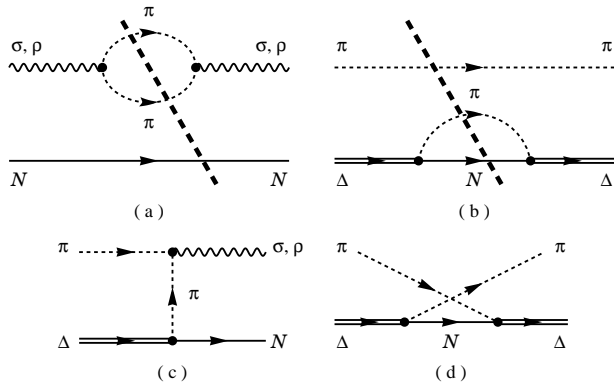


FIG. 3: Diagrams for the $\pi\pi N$ three-body unitary cut. (a) and (b) are taken into account in the present model, while (c) and (d) are not included.

is necessary to include the so-called Z diagrams, which corresponds to Figs. 3(c) and 3(d), in addition to the usual two-body to two-body interaction terms [51].

D. Bare N^* and Δ^* states

Now I introduce bare N^* and Δ^* states, which are embedded into the πN coupled-channels interactions. They are described as s -channel interactions

$$V_{jk}^{\text{bare}}(E; q', q) = \frac{g_j g_k}{2m_\pi(E - M_0)} \left(\frac{q'}{m_\pi}\right)^{L'} \left(\frac{q}{m_\pi}\right)^L \times \mathcal{F}(\Lambda, q') \mathcal{F}(\Lambda, q). \quad (42)$$

These interactions are added to each partial-wave component of the πN coupled-channels interaction V in Eq. (1). Here M_0 is the bare mass, g_j is the coupling constant of the bare state to the channel j , form factor \mathcal{F} is the same as in Eq. (36), and $L^{(\prime)}$ is the orbital angular momentum of the initial (final) meson-baryon state. The bare mass M_0 , coupling constant g_j , and cutoff Λ are free parameters and are fixed in the fits. I use a single cutoff Λ for each N^* or Δ^* state to reduce the number of parameters.

Because the bare-state contributions are implemented into the two-body coupled-channels interactions as in Eq. (42), they depend on the energy E , which will bring

nonzero missing-channel contribution Z (15) corresponding to the implicit bare states [23].

A problem is to specify the number of bare N^* and Δ^* states in each partial wave. In the present study I take into account the bare states only if the bare states can significantly improve the fitting and reproduce well resonance-like behaviors of the on-shell πN amplitudes. In this strategy I introduce the bare N^* and Δ^* states listed in Table III, in which the fitted values of the parameters are shown as well.

E. Fit to the experimental πN amplitudes

The present model for the πN coupled-channels amplitudes contains the model parameters: coupling constants, cutoffs, and bare-state masses. They can be determined by fitting the experimental data of the on-shell πN scattering amplitudes. In the present study, while I fix the cutoffs for the meson-meson-meson vertices as $\Lambda_{\pi\pi\rho} = \Lambda_{\pi\pi\sigma} = 1000$ MeV, I allow the other model parameters to vary freely so as to reproduce the on-shell πN scattering amplitudes. The fixed value $\Lambda_{\pi\pi\rho} = \Lambda_{\pi\pi\sigma} = 1000$ MeV is a typical value of the hadronic scale, and I checked that the on-shell πN scattering amplitudes only weakly depend on the meson-meson-meson cutoffs $\Lambda_{\pi\pi\rho}$, $\Lambda_{\pi\pi\sigma}$.

For the on-shell πN scattering amplitudes, I employ the database of SAID [48]. Restricting the center-of-mass energy $E \leq 1.9$ GeV and orbital angular momentum $L \leq 2$, I obtain the model parameters listed in Tables III and IV by the fitting.

The results of the on-shell πN amplitudes are shown in

TABLE IV: Fitted values of coupling constants and cutoff parameters. Cutoff parameters are in units of MeV.

$f_{\pi N \Delta}$	-0.439	$\Lambda_{\pi NN}$	566
$g_{\pi\pi\rho}$	2.876	$\Lambda_{\pi N \Delta}$	510
$g_{\rho NN}$	8.783	$\Lambda_{\pi\pi\rho}$	1000
κ_ρ	4.806	$\Lambda_{\rho NN}$	564
$g_{\pi\pi\sigma}$	3.188	$\Lambda_{\pi\pi\sigma}$	1000
$g_{\sigma NN}$	21.571	$\Lambda_{\sigma NN}$	564
		$\Lambda_{\eta NN}$	843

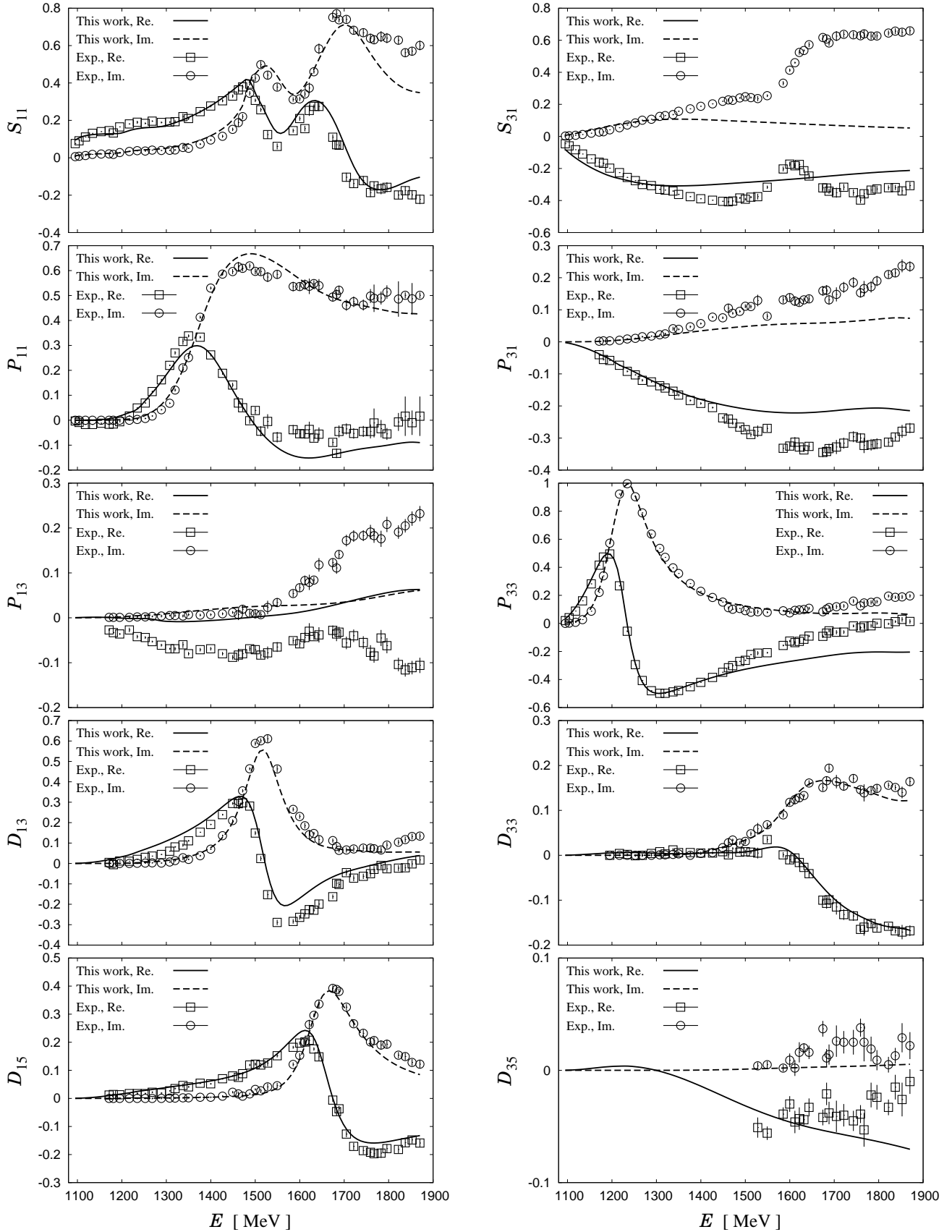


FIG. 4: Fitted πN scattering amplitudes L_{2I2J} . Lines (points) represent results of the present calculation (SAID analysis [48]).

TABLE V: Nucleon resonances obtained in this study. I here show their pole positions in the present model E_{pole} and their locations in terms of the Riemann sheets, pole positions listed in Particle Data Group (PDG) [1], compositeness X (25), missing-channel contributions Z (15), uncertainties U (17) and U_r (20), and real-valued quantities \tilde{X} and \tilde{Z} (18). The notation of the pole locations is explained in the text. The indices 1, 2, 3 (1, 2) for the ρN ($\pi\Delta$) channel represent the same order as in Table I.

	$N(1535) 1/2^-$	$N(1650) 1/2^-$	$N(1440)_1 1/2^+$	$N(1440)_2 1/2^+$
E_{pole} [MeV]	1527 - 45 <i>i</i>	1699 - 70 <i>i</i>	1362 - 106 <i>i</i>	1361 - 114 <i>i</i>
Location	(22111)	(22112)	(21112)	(21111)
E_{pole} (PDG) [MeV]	(1500-1520) - (55-75) <i>i</i>	(1640-1670) - (50-85) <i>i</i>	(1360-1380) - (80-95) <i>i</i>	(1360-1380) - (80-95) <i>i</i>
$X_{\pi N}$	-0.09 + 0.01 <i>i</i>	-0.05 - 0.02 <i>i</i>	0.47 + 0.35 <i>i</i>	0.55 + 0.28 <i>i</i>
$X_{\eta N}$	-0.42 - 0.19 <i>i</i>	-0.02 - 0.01 <i>i</i>	-0.00 - 0.01 <i>i</i>	-0.00 - 0.01 <i>i</i>
$X_{\sigma N}$	-0.00 + 0.03 <i>i</i>	-0.00 + 0.09 <i>i</i>	0.40 + 0.15 <i>i</i>	0.46 + 0.03 <i>i</i>
$X_{\rho N(1)}$	0.37 - 0.09 <i>i</i>	0.21 - 0.60 <i>i</i>	-0.00 + 0.00 <i>i</i>	-0.00 + 0.00 <i>i</i>
$X_{\rho N(2)}$	0.31 - 0.00 <i>i</i>	0.09 - 0.01 <i>i</i>	-0.00 - 0.03 <i>i</i>	-0.01 - 0.03 <i>i</i>
$X_{\pi\Delta(1)}$	0.06 - 0.01 <i>i</i>	0.07 + 0.12 <i>i</i>	0.03 - 0.24 <i>i</i>	0.02 - 0.06 <i>i</i>
Z	0.78 + 0.25 <i>i</i>	0.71 + 0.43 <i>i</i>	0.11 - 0.23 <i>i</i>	-0.01 - 0.22 <i>i</i>
U	1.15	0.87	0.55	0.40
U_r	0.16	0.12	0.08	0.06
$\tilde{X}_{\pi N}$	0.04	0.03	0.38	0.44
$\tilde{X}_{\eta N}$	0.22	0.01	0.00	0.00
$\tilde{X}_{\sigma N}$	0.01	0.05	0.28	0.33
$\tilde{X}_{\rho N(1)}$	0.18	0.34	0.00	0.00
$\tilde{X}_{\rho N(2)}$	0.14	0.05	0.02	0.02
$\tilde{X}_{\pi\Delta(1)}$	0.03	0.08	0.15	0.05
\tilde{Z}	0.38	0.44	0.17	0.16

	$N(1520) 3/2^-$	$N(1675) 5/2^-$	$\Delta(1232) 3/2^+$	$\Delta(1700) 3/2^-$
E_{pole} [MeV]	1506 - 53 <i>i</i>	1652 - 57 <i>i</i>	1216 - 54 <i>i</i>	1666 - 84 <i>i</i>
Location	(22112)	(22 - 12)	(2 - - 11)	(2 - - 12)
E_{pole} (PDG) [MeV]	(1505-1515) - (52.5-60) <i>i</i>	(1655-1665) - (62.5-75) <i>i</i>	(1209-1211) - (49-51) <i>i</i>	(1640-1690) - (100-150) <i>i</i>
$X_{\pi N}$	0.05 + 0.16 <i>i</i>	-0.03 + 0.05 <i>i</i>	-0.03 + 0.59 <i>i</i>	-0.03 + 0.00 <i>i</i>
$X_{\eta N}$	0.01 - 0.00 <i>i</i>	0.06 + 0.24 <i>i</i>		
$X_{\sigma N}$	0.15 + 0.11 <i>i</i>			
$X_{\rho N(1)}$	0.01 - 0.06 <i>i</i>	0.01 - 0.00 <i>i</i>	0.00 - 0.00 <i>i</i>	0.48 - 0.09 <i>i</i>
$X_{\rho N(2)}$	0.04 - 0.02 <i>i</i>	0.02 - 0.01 <i>i</i>	0.01 + 0.00 <i>i</i>	0.05 - 0.02 <i>i</i>
$X_{\rho N(3)}$	0.08 - 0.04 <i>i</i>			0.09 - 0.02 <i>i</i>
$X_{\pi\Delta(1)}$	-0.00 + 0.00 <i>i</i>	0.08 + 0.07 <i>i</i>	0.00 - 0.00 <i>i</i>	-0.08 - 0.23 <i>i</i>
$X_{\pi\Delta(2)}$	0.02 - 0.00 <i>i</i>			-0.01 + 0.04 <i>i</i>
Z	0.62 - 0.15 <i>i</i>	0.86 - 0.35 <i>i</i>	1.02 - 0.59 <i>i</i>	0.50 + 0.31 <i>i</i>
U	0.24	0.37	0.77	0.54
U_r	0.03	0.06	0.15	0.08
$\tilde{X}_{\pi N}$	0.14	0.04	0.33	0.02
$\tilde{X}_{\eta N}$	0.01	0.18		
$\tilde{X}_{\sigma N}$	0.15			
$\tilde{X}_{\rho N(1)}$	0.05	0.01	0.00	0.32
$\tilde{X}_{\rho N(2)}$	0.04	0.02	0.01	0.03
$\tilde{X}_{\rho N(3)}$	0.08			0.06
$\tilde{X}_{\pi\Delta(1)}$	0.00	0.08	0.00	0.16
$\tilde{X}_{\pi\Delta(2)}$	0.02			0.03
\tilde{Z}	0.51	0.67	0.66	0.39

Fig. 4. As one can see, the present model reproduces the on-shell πN amplitudes fairly well except for the S_{31} , P_{31} , and P_{13} amplitudes. In particular, the resonance-like behavior in S_{11} , P_{11} , P_{33} , D_{13} , D_{33} , and D_{15} is well reproduced. Indeed, fittings to these amplitudes are significantly improved by introducing two bare N^* states in

the S_{11} and one bare N^* or Δ^* state in the P_{11} , P_{33} , D_{13} , D_{33} , and D_{15} , respectively.

On the other hand, I can quantitatively reproduce the S_{31} and P_{31} amplitudes only in the low-energy region $E \lesssim 1250$ MeV. For the P_{13} amplitude, I can only reproduce the smallness of the absolute value of the amplitude

($\lesssim 0.1$). I expect that one could cure these discrepancies in the S_{31} , P_{31} , and P_{13} amplitudes by employing further diagrams of the meson–baryon interactions or phenomenological contact potentials as done in Ref. [6] for the S_{31} partial wave, and by taking into account other meson–baryon channels such as $K\Lambda$ and $K\Sigma$. I note that, although the experimental data imply resonances around 1600 MeV and 1700 MeV in the S_{31} and P_{13} , respectively, I do not include bare states in these partial waves because bare states will not significantly improve the fittings.

IV. THE MESON–BARYON COMPOSITENESS FOR THE N^* AND Δ^* RESONANCES

In this section I calculate the compositeness of the πN , ηN , σN , ρN , and $\pi\Delta$ channels for the N^* and Δ^* resonances.

One of the most interesting features in hadron physics is the competition between hadron degrees of freedom and quark degrees of freedom. In the present N^*/Δ^* case, bare states which are expected to originate from quark degrees of freedom are embedded into the πN coupled channels. As a consequence, even if a meson–baryon interaction is strongly attractive enough to make a bound state, the bound state is in general contaminated by bare N^*/Δ^* states which couple to the meson–baryon system. Conversely, it is inevitable that a bare N^*/Δ^* state is dressed in meson–baryon clouds. The compositeness is applicable to evaluating both the dominance of the meson–baryon molecular components and the fractions of the meson–baryon clouds for physical nucleon resonances.

In the present study, I employ the interaction diagrams in Fig. 1 and several bare N^* and Δ^* states for the πN coupled-channels scattering, and fix the model parameters so as to reproduce the on-shell πN amplitude, as explained in the previous section. I perform the analytic continuations of the scattering amplitudes to the complex energy plane in the complex scaling method, and find resonance poles corresponding to the $N(1535)$ and $N(1650)$ in the spin/parity $J^P = 1/2^-$, $N(1440)$ in $1/2^+$, $N(1520)$ in $3/2^-$, $N(1675)$ in $5/2^-$, $\Delta(1232)$ in $3/2^+$, and $\Delta(1700)$ in $3/2^-$, where the names are taken from Particle Data Group (PDG) [1]. Their pole positions are listed in Table V together with the results of the compositeness X (25), missing-channel contributions Z (15), uncertainties U (17) and U_r (20), and real-valued quantities \tilde{X} and \tilde{Z} (18).

Below I discuss the internal structure of the N^* and Δ^* resonances on their resonance poles.

A. $N(1440)$

The $N(1440)$ resonance in $J^P = 1/2^+$, also known as the Roper resonance, is one of the most interesting

states among the nucleon resonances. The Roper resonance is lighter than the lowest negative-parity nucleon excitations, i.e., $N(1535)$ in $J^P = 1/2^-$ and $N(1520)$ in $J^P = 3/2^-$, which cannot be easily explained if one assumes that the Roper resonance is a radial excitation of nucleon as a three-quark system. A promising physical interpretation is that the Roper resonance is the first radial excitation of nucleon but consists of a dressed-quark core augmented by a meson cloud [52]. Importance of the contribution from the πN coupled-channels dynamics was also pointed out in, e.g., Refs. [3, 9, 11, 13, 53, 54]. In this sense, the use of the two-body wave functions and compositeness in my approach is quite suitable for studying the internal structure of the Roper resonance.

In the present πN coupled-channels model, I find two poles of the scattering amplitude corresponding to the Roper resonance at $E_{\text{pole}} = 1362 - 106i$ MeV and $1361 - 114i$ MeV. The pole positions deviate only slightly from the value reported by PDG. The former pole is found with the complex-scaling angle $\theta \geq 45^\circ$ in the complex scaling method. This indicates that the former pole exists in the second Riemann sheets of the πN and $\pi\Delta$ channels but in the first Riemann sheets of the ηN , σN , and ρN channels (see Fig. 2), to which I refer as (21112) in the order πN , ηN , σN , ρN , and $\pi\Delta$. On the other hand, the latter pole is found with the scaling angle $25^\circ \leq \theta \leq 40^\circ$, and hence it exists in the sheet (21111). Because the former pole is closer to the physical region, i.e., the real energy axis, the former is the resonance pole for the Roper resonance and write it as $N(1440)_1$. On the other hand, the latter pole is the shadow pole for the Roper resonance [53] and write it as $N(1440)_2$. I note that the pole positions E_{pole} do not depend on the scaling angle θ but one can switch the Riemann sheets at a certain energy by varying θ .

From the residues of the off-shell scattering amplitudes at the poles, I can calculate the two-body wave functions and compositeness as their norms both for the $N(1440)_1$ and $N(1440)_2$, according to the method in Sec. II. The results of the compositeness X_j (25) of the j th meson–baryon channel and missing-channel contribution Z (15) are listed in Table V. I checked that the compositeness does not depend on the scaling angle θ . As one can see from the Table, although the values of the compositeness are complex due to the resonance nature, the real parts of $X_{\pi N}$ and $X_{\sigma N}$ for the both poles are as large as 0.5, which should be compared with unity, and their imaginary parts are smaller than the real parts. On the other hand, the missing-channel contribution Z is close to zero. Because the nonzero value of Z comes from the bare state in the meson–baryon interaction (42) as well as the $\pi\pi N$ state in the self-energies of Eqs. (39)–(41), the present result strongly implies that, while the πN and σN molecular components dominate both the $N(1440)_1$ and $N(1440)_2$ states as “thick meson clouds”, the bare-state contribution is small.

The complex-valued compositeness, however, cannot be interpreted as probabilities of finding meson–baryon

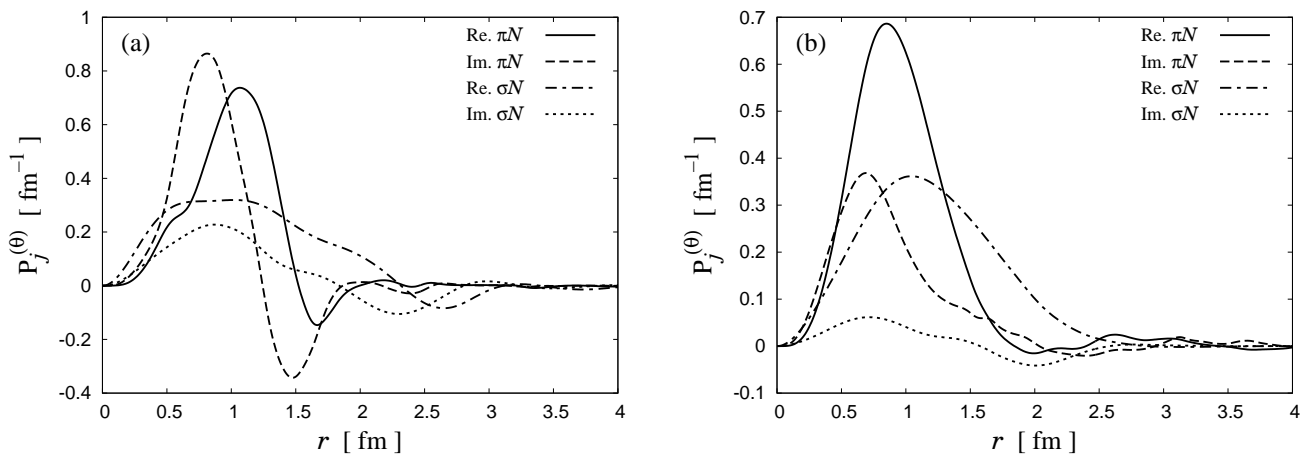


FIG. 5: Density distributions of the πN and σN components for the $N(1440)$ resonance in coordinate space. (a) For the $N(1440)_1$ pole with the complex-scaling angle $\theta = 50^\circ$. (b) For the $N(1440)_2$ pole with the complex-scaling angle $\theta = 35^\circ$.

components. To draw a more definite conclusion, I calculate the real-valued quantities \tilde{X} and \tilde{Z} (18) together with U (17) and U_r (20) for the $N(1440)_1$ and $N(1440)_2$ states. The results are listed in Table V. The value of the reduced uncertainty U_r is smaller than 0.1 for both poles. Therefore, according to the discussions in the end of Sec. II A, I can interpret \tilde{X}_j (\tilde{Z}) as the probability of finding the composite (missing) part with small uncertainties. From the values in Table V, I can conclude more definitely that the πN and σN molecular components, whose contributions are almost the same as each other, dominate the $N(1440)_1$ and $N(1440)_2$ states while the bare-state contribution is about less than 20% in the present model. These findings are consistent with the previous studies in, e.g., Refs. [3, 9, 11, 13, 52–54], in which a significant contribution from meson–baryon coupled channels was reported. In particular, the present study supports the scenario drawn in Ref. [3] that the $\pi N \rightarrow \sigma N$ transition potential and treatment of the $\pi\pi N$ components in the unstable σN channel are important for the description of the Roper resonance.

The squared wave functions in coordinate space (27) represent the behavior of relative motions between the mesons and baryons as the density distributions. The density distributions $P_j^{(\theta)}$ for the $N(1440)_1$ and $N(1440)_2$ states are plotted in Fig. 5 as functions of the relative distance r between the mesons and baryons. The scaling angle is fixed as $\theta = 50^\circ$ for the $N(1440)_1$ and $\theta = 35^\circ$ for the $N(1440)_2$. Although the density distributions are complex for resonances in general and depend on θ , they provide information on the typical distance between the mesons and baryons. The results of the density distributions imply that both in the πN and σN channels the meson–baryon separation is about more than 1 fm for the $N(1440)_1$ and $N(1440)_2$ states.

B. $\Delta(1232)$

The $\Delta(1232)$ resonance in $J^P = 3/2^+$ is also interesting, because there are several suggestions of its large πN component. Historically, it was pointed out in Ref. [55] that the $\Delta(1232)$ resonance can occur by the attractive p -wave πN interaction. A hint of the large effect of the meson cloud is seen, for instance, in the $M1$ transition form factor for $\gamma^* N \rightarrow \Delta$ at $Q^2 = 0$ [56]. Further studies on the dynamical generation of the $\Delta(1232)$ resonance can be seen, e.g., in Refs. [28, 31, 57]. I can examine the picture of a large πN component in terms of the compositeness.

In the present model, I observe the resonance pole for the $\Delta(1232)$ at $1216 - 54i$ MeV in the Riemann sheet (2 - - 11), where hyphen represents a decoupled channel. The compositeness calculated from the residue and pole position for the $\Delta(1232)$ is listed in Table V. The πN compositeness $X_{\pi N}$ has nonnegligible imaginary part but its real part is small. The other meson–baryon channels, i.e., the $\rho N(L = 1, S = 1/2)$, $\rho N(L = 1, S = 3/2)$, and $\pi\Delta$ channels give negligible contributions to the compositeness, and hence the missing-channel contribution Z is almost unity in the real part and negatively large in the imaginary part. Because the bare Δ^* state exists near the physical pole position, I can expect that Z is dominated by the bare state. Therefore, the results imply that the bare-state contribution is the most essential for the physical $\Delta(1232)$ resonance. Nevertheless, I expect that the large absolute value $|X_{\pi N}|$ reflects the importance of the πN channel in the $\Delta(1232)$ and affects the properties of the $\Delta(1232)$ as the meson clouds.

Besides, the reduced uncertainty U_r is as large as 0.15 owing to the large imaginary part in the πN channel. Therefore, although $\tilde{X}_{\pi N}$ takes a nonnegligible value ~ 0.3 , I cannot definitely interpret it as the probability of finding πN component inside the $\Delta(1232)$ resonance.

C. $N(1535)$, $N(1650)$, $N(1520)$, $N(1675)$, and $\Delta(1700)$

Next I consider the other resonances: $N(1535)$ and $N(1650)$ in $J^P = 1/2^-$, $N(1520)$ in $3/2^-$, $N(1675)$ in $5/2^-$, and $\Delta(1700)$ in $3/2^-$. The results of their pole positions and compositeness are listed in Table V.

The $N(1535)$ and $N(1650)$ resonances exist in the Riemann sheets (22111) and (22112), respectively. The results of the compositeness for the $N(1535)$ imply that the bare-state contribution is dominant but the coupling to the ηN channel, whose branch point is the closest to the $N(1535)$ pole position, would be large. However, the real part of the ηN compositeness $X_{\eta N}$ is negatively large, which is canceled with the real parts of the ρN compositeness. As a consequence, the reduced uncertainty U_r is as large as $\tilde{X}_{\eta N, \rho N(1), \rho N(2)}$ for the $N(1535)$ and I cannot interpret $\tilde{X}_{\eta N, \rho N(1), \rho N(2)}$ as the probabilities of finding the ηN and ρN components, respectively.

On the other hand, for the $N(1650)$, because $U_r = 0.12$, I can interpret $\tilde{X}_{\rho N(1)}$ and \tilde{Z} as the probabilities with uncertainties ~ 0.1 . The results of \tilde{X}_j and \tilde{Z} indicate that about half of the $N(1650)$ comes from missing channels, in the present case the bare state, while it has a certain fraction of the $\rho N(L=0, S=1/2)$ cloud.

Similarly, the poles of the $N(1520)$, $N(1675)$, and $\Delta(1700)$ resonances are found in the (22112), (22 - 12), and (2 - - 12) Riemann sheets, respectively. The results of the compositeness indicate that they are dominated by missing channels, i.e., the bare states. The $\Delta(1700)$ resonance has a certain fraction of the $\rho N(L=0, S=3/2)$ cloud, while the $N(1520)$ and $N(1675)$ resonances have only small fractions of meson–baryon clouds.

These results indicate that, although the $N(1535)$, $N(1650)$, $N(1520)$, $N(1675)$, and $\Delta(1700)$ resonances have some fractions of the meson–baryon clouds, they do not have dominant meson–baryon molecular components. The largest fractions of the meson–baryon clouds are the ρN for the $N(1650)$ and $\Delta(1700)$ resonances, which amount to ~ 0.3 with uncertainties ~ 0.1 . These are because the resonance pole positions are close to the ρN branch point and coupling constants of the N^*/Δ^* bare states to the ρN channel are large, as seen in Table III.

V. CONCLUSION

In this study I have investigated the internal structure of the nucleon resonances N^* and Δ^* in terms of the meson–baryon two-body wave functions and compositeness. One of the most essential parts in my approach is to extract the meson–baryon two-body wave functions by using the pole positions for the nucleon resonances in the complex energy plane of the πN coupled-channels scattering amplitudes and residues for them. Here the scattering amplitudes are solutions of the Lippmann–

Schwinger equation. In this strategy, for each resonance pole I can obtain wave functions of the πN and coupled channels which are automatically scaled, thanks to the inhomogeneous property of the Lippmann–Schwinger equation. As a consequence, by calculating the compositeness, which is defined as the norm of the two-body wave function from the meson–baryon scattering amplitudes, and by comparing the compositeness with unity, I can evaluate the dominance of the meson–baryon molecular components as well as the fractions of meson–baryon clouds for physical nucleon resonances.

For this purpose I have constructed a meson exchange model in a πN - ηN - σN - ρN - $\pi \Delta$ coupled-channels problem and involve several bare N^* and Δ^* states. The coupling constants, cutoffs, and bare-state masses as the model parameters were fixed so as to reproduce the experimental data of the on-shell πN scattering amplitudes in the center-of-mass energy $E \leq 1.9$ GeV and orbital angular momentum $L \leq 2$. The constructed model reproduced the on-shell πN amplitudes fairly well and generated resonance poles corresponding to the $N(1535)$ and $N(1650)$ in the spin/parity $J^P = 1/2^-$, $N(1440)$ in $1/2^+$, $N(1520)$ in $3/2^-$, $N(1675)$ in $5/2^-$, $\Delta(1232)$ in $3/2^+$, and $\Delta(1700)$ in $3/2^-$ in the complex energy plane of the scattering amplitudes. In the present model the Roper resonance $N(1440)$ is composed of two poles in different $\pi \Delta$ sheets.

Then I have calculated the meson–baryon wave functions and compositeness from the scattering amplitudes for these nucleon resonances. As a result, the Roper resonance $N(1440)$, for both the two poles, was found to be dominated by the πN and σN molecular components, whose contributions are almost the same as each other, while the bare-state contribution is about less than 20% in the present model. The squared wave functions in coordinate space imply that both in the πN and σN channels the separation between the meson and baryon is about more than 1 fm for the $N(1440)$ resonance. On the other hand, dominant meson–baryon molecular components were not observed in any other N^* and Δ^* resonances in the present model, although they have some fractions of the meson–baryon clouds.

Here I emphasize that the present strategy to calculate the compositeness is in general applicable as long as the Lippmann–Schwinger equation is fully solved for hadron–hadron scatterings. In this sense, more definitely conclusion about the composite nature of nucleon resonances will be drawn with more sophisticated models such as Refs. [5, 6, 21], in which they precisely reproduced experimental data of not only the on-shell πN amplitudes but also the pion- and photon-induced reactions. Furthermore, excited baryons with non-zero strangeness, i.e., Λ^* , Σ^* , Ξ^* , and Ω^* states, will be important as a next target, because they will be discovered and be investigated extensively in near future experiments at J-PARC, JLab, etc., as well as in the relativistic heavy ion collisions. To construct scattering amplitudes for these resonances, approaches in, e.g., Refs. [58, 59] will be helpful.

Finally I comment on the model dependence of the two-body wave functions and compositeness. Because the compositeness as well as the wave functions is not observable, the compositeness is in general a model dependent quantity. This fact has a special meaning when one discusses a hadron–hadron molecular component in a hadron resonance. The strong interactions between hadrons emerge as a nonperturbative phenomenon of the underlying theory, QCD, and hence one cannot obtain the strong interactions between hadrons by analytically solving QCD. This is in contrast to the electromagnetic case, in which the electromagnetic interactions can be directly obtained by the fundamental theory, quantum electrodynamics (QED). Therefore, to pin down the hadron–hadron interaction and calculate its off-shell part, which plays an essential role in the two-body wave functions and compositeness, we have to fix a scheme based on a certain principle such as meson exchanges and employ effective Lagrangians which govern the hadron–hadron interaction. The present article indeed suggests a strategy in this line to elucidate the internal structure of hadron resonances in terms of the hadron–hadron molecular components.

Acknowledgments

The author acknowledges H. Kamano, S. X. Nakamura, and T. Sato for helpful discussions on the πN partial-wave analysis and on the N^* and Δ^* physics. He is also very grateful to D. Jido and T. Hyodo for fruitful discussions on the compositeness. This work is partly supported by JSPS KAKENHI Grant No. JP15K17649.

Appendix A: Masses of hadrons

In this study I employ isospin symmetric masses for hadrons: $m_\pi = 138.0 \text{ MeV}$, $m_\eta = 547.9 \text{ MeV}$, and $m_N = 938.9 \text{ MeV}$. These values are used in the t -channel pion propagators and in the s - and u -channel nucleon propagators as well as in the initial and final states. The masses in the unstable initial and final states are taken from the bare states in the self-energies: $m_{\sigma_0} = 700 \text{ MeV}$, $m_{\rho_0} = 812 \text{ MeV}$, and $m_{\Delta_0} = 1280 \text{ MeV}$. The value $m_{\sigma_0} = 700 \text{ MeV}$ is used for the t -channel σ exchange in the $\pi N \rightarrow \pi N$ interaction, while physical values $m_\rho = 775.3 \text{ MeV}$ and $m_\Delta = 1210 \text{ MeV}$ are used for the t -channel ρ exchange and u -channel Δ exchange in the $\pi N \rightarrow \pi N$ interaction, respectively.

Appendix B: Partial waves of the meson–baryon interactions

In this Appendix I summarize the notations and partial-wave projections of the meson–baryon (MB) interactions.

1. Notations

The meson–baryon scatterings are denoted by $M(k^\mu, \lambda_M)B(p^\mu, \lambda_B) \rightarrow M'(k'^\mu, \lambda_{M'})B'(p'^\mu, \lambda_{B'})$, where $k^{(\prime)\mu}$ and $p^{(\prime)\mu}$ are momenta and $\lambda_{M,B}$ are helicities of the meson and baryon, respectively. Since I consider scatterings in the center-of-mass frame, I can write the three-momenta as $\mathbf{q} \equiv \mathbf{k} = -\mathbf{p}$ and $\mathbf{q}' \equiv \mathbf{k}' = -\mathbf{p}'$. Without loss of generality, I can choose the coordinates such that

$$\mathbf{q} = (0, 0, q), \quad \mathbf{q}' = (q' \sin \theta, 0, q' \cos \theta), \quad (\text{B1})$$

with the scattering angle θ . The masses of the meson $M^{(\prime)}$ and baryon $B^{(\prime)}$ are expressed as $m_{M^{(\prime)}}$ and $m_{B^{(\prime)}}$, respectively. Throughout this study I fix the energies of the four-momenta k^μ and p^μ to their on-shell values as

$$k^0 = \sqrt{m_M^2 + q^2}, \quad p^0 = \sqrt{m_B^2 + q^2}, \quad (\text{B2})$$

and similarly for k'^0 and p'^0 .

2. Partial-wave projections

I calculate the partial-wave matrix elements of the interaction V_α by following the Jacob–Wick formulation [60], where α specifies the quantum numbers of the system. In the πN coupled-channels scattering case, I take $\alpha = (J^P, I)$ with the total angular momentum J , parity P , and isospin I .

First, according to Feynman diagrams, I calculate the interactions in terms of the helicity eigenstates

$$V_{MB \rightarrow M'B'} = V_{MB \rightarrow M'B'}(\mathbf{q}', \lambda_{M'}, \lambda_{B'}, \mathbf{q}, \lambda_M, \lambda_B). \quad (\text{B3})$$

Then, the interactions are projected to the total angular momentum J as

$$\begin{aligned} V^J(q', \lambda_{M'}, \lambda_{B'}, q, \lambda_M, \lambda_B) \\ = 2\pi \int_{-1}^1 d \cos \theta d_{\lambda_M - \lambda_B, \lambda_{M'} - \lambda_{B'}}^J(\theta) \\ \times V(\mathbf{q}', \lambda_{M'}, \lambda_{B'}, \mathbf{q}, \lambda_M, \lambda_B), \end{aligned} \quad (\text{B4})$$

where I omitted the subscript $MB \rightarrow M'B'$ of V , and $d_{m' m}^j$ is the Wigner d -matrix.

The interaction of the total angular momentum J is projected to the states with definite orbital angular momenta and spins for the meson–baryon channels as

$$\begin{aligned} V_\alpha(q', q) = \kappa(q', q) \sum_{\lambda_M, \lambda_B, \lambda_{M'}, \lambda_{B'}} \frac{\sqrt{(2L+1)(2L'+1)}}{2J+1} \\ \times \langle j_{M'} j_{B'} \lambda_{M'} - \lambda_{B'} | S' S'_z \rangle \langle L' S' 0 S'_z | J S'_z \rangle \\ \times \langle j_M j_B \lambda_M - \lambda_B | S S_z \rangle \langle L S 0 S_z | J S_z \rangle \\ \times V^J(q', \lambda_{M'}, \lambda_{B'}, q, \lambda_M, \lambda_B), \end{aligned} \quad (\text{B5})$$

TABLE VI: Isospin factors for the interactions.

	$I = 1/2$	$I = 3/2$
$\tau^j \tau^i$	3	0
$\tau^i \tau^j$	-1	2
δ_{ij}	1	1
$i\epsilon_{jik} \tau^k$	2	-1
$T^i T^{\dagger j}$	4/3	1/3
τ^i	$-\sqrt{3}$	0
τ^j	$-\sqrt{3}$	0
$T^{\dagger j} \tau^i$	$\sqrt{6}$	0
$T^{\dagger i} \tau^j$	$\sqrt{8/3}$	$-\sqrt{5/3}$
$T^{\dagger j}$	$-\sqrt{2}$	0
$T^{\dagger j} T^i$	2	0

where $j_{M^{(\prime)}}$ and $j_{B^{(\prime)}}$ are the spins of the meson $M^{(\prime)}$ and baryon $B^{(\prime)}$, respectively, $L^{(\prime)}$ and $S^{(\prime)}$ are the orbital angular momentum and spin in the initial (final) state, respectively, $S_z \equiv \lambda_M - \lambda_B$, and $S'_z \equiv \lambda_{M'} - \lambda_{B'}$. $\langle j_M j_B \lambda_M - \lambda_B | S S_z \rangle$ is the Clebsch–Gordan coefficient. The factor $\kappa(q', q)$, which is defined as

$$\kappa(q', q) \equiv \frac{1}{(2\pi)^3} \sqrt{\frac{m_B m_{B'}}{4\omega_M(q) E_B(q) \omega_{M'}(q') E_{B'}(q')}}}, \quad (\text{B6})$$

with $\omega_{M^{(\prime)}}(q) \equiv \sqrt{q^2 + m_{M^{(\prime)}}^2}$ and $E_{B^{(\prime)}}(q) \equiv \sqrt{q^2 + m_{B^{(\prime)}}^2}$, was introduced so as to satisfy the opti-

cal theorem with the correct coefficients. The interaction (B5) is applicable to the Lippmann–Schwinger equation (1).

Appendix C: Explicit forms of the meson–baryon interactions

In this Appendix I show the explicit forms of the interactions $M(k^\mu, \lambda_M) B(p^\mu, \lambda_B) \rightarrow M'(k'^\mu, \lambda_{M'}) B'(p'^\mu, \lambda_{B'})$ used in the present study. The interactions are written in terms of the helicity eigenstates, i.e., those in Eq. (B3), except for the s -channel contributions of the bare N^* and Δ^* states in Appendix C 16.

For the incoming and outgoing nucleons, I express the helicity eigenstates by the Dirac spinors $u_N(-\mathbf{q}, \lambda_N)$ and $\bar{u}_N(-\mathbf{q}', \lambda_{N'})$, respectively. The spinors for the incoming and outgoing ρ meson are $e_\rho^\mu(\mathbf{q}, \lambda_M)$ and $e_\rho^{\mu*}(\mathbf{q}', \lambda_{M'})$, respectively. The helicity eigenstates of the Δ baryon as the Rarita-Schwinger spinor are $u_\Delta^\mu(-\mathbf{q}, \lambda_\Delta)$ for the incoming and $\bar{u}_\Delta^\mu(-\mathbf{q}', \lambda_{\Delta'})$ for the outgoing states. The explicit forms of the spinors are given in Ref. [61].

In this study I multiply a factor i for the incoming σ and ρ mesons and accordingly a factor $-i$ for the outgoing σ and ρ mesons to obtain a real-valued interaction.

1. $\pi N \rightarrow \pi N$

The $\pi^i N \rightarrow \pi^j N$ interactions, where the isospin indices for mesons $i, j = 1, 2, 3$ correspond to those in Eq. (30), are given as

$$V_{\pi N \rightarrow \pi N} = \bar{u}_N(-\mathbf{q}', \lambda_{N'}) (\bar{V}_{1a} + \bar{V}_{1b} + \bar{V}_{1c} + \bar{V}_{1d} + \bar{V}_{1e}) u_N(-\mathbf{q}, \lambda_N), \quad (\text{C1})$$

with

$$\bar{V}_{1a} = (\tau^j \tau^i) \left(\frac{D+F}{2f_\pi} \right)^2 \not{k}' \gamma_5 \frac{S_N(p+k) + S_N(p'+k')}{2} \not{k} \gamma_5 \mathcal{F}(\Lambda_{\pi NN}, q') \mathcal{F}(\Lambda_{\pi NN}, q), \quad (\text{C2})$$

$$\bar{V}_{1b} = (\tau^i \tau^j) \left(\frac{D+F}{2f_\pi} \right)^2 \not{k} \gamma_5 \frac{S_N(p-k') + S_N(p'-k)}{2} \not{k}' \gamma_5 \mathcal{F}(\Lambda_{\pi NN}, q') \mathcal{F}(\Lambda_{\pi NN}, q), \quad (\text{C3})$$

$$\bar{V}_{1c} = (T^i T^{\dagger j}) \left(\frac{f_{\pi N \Delta}}{m_\pi} \right)^2 k_\mu \left[\frac{S_\Delta^{\mu\nu}(p-k') + S_\Delta^{\mu\nu}(p'-k)}{2} \right] k'_\nu \mathcal{F}(\Lambda_{\pi N \Delta}, q') \mathcal{F}(\Lambda_{\pi N \Delta}, q), \quad (\text{C4})$$

$$\begin{aligned} \bar{V}_{1d} = & (i\epsilon_{jik} \tau^k) \frac{g_{\pi\pi\rho} g_{\rho NN}}{2} \left[\frac{S_\rho(k-k') + S_\rho(p'-p)}{2} \right] \\ & \times \left\{ \not{k} + \not{k}' + \frac{\kappa_\rho}{4m_N} [(\not{k} + \not{k}')(\not{p} - \not{p}') - (\not{p} - \not{p}')(\not{k} + \not{k}')] \right\} \mathcal{F}(\Lambda_{\pi\pi\rho}, |\mathbf{q} - \mathbf{q}'|) \mathcal{F}(\Lambda_{\rho NN}, |\mathbf{q} - \mathbf{q}'|), \end{aligned} \quad (\text{C5})$$

$$\bar{V}_{1e} = (\delta_{ij}) \left(-\frac{g_{\pi\pi\sigma} g_{\sigma NN}}{m_\pi} \right) k^\mu k'_\mu \left[\frac{S_\sigma(k-k') + S_\sigma(p'-p)}{2} \right] \mathcal{F}(\Lambda_{\pi\pi\sigma}, |\mathbf{q} - \mathbf{q}'|) \mathcal{F}(\Lambda_{\sigma NN}, |\mathbf{q} - \mathbf{q}'|). \quad (\text{C6})$$

The explicit values of the isospin factors are listed in Table VI. Propagators S_N , S_Δ , S_ρ , and S_σ are respectively:

$$\begin{aligned} S_N(p) &= \frac{\not{p} + m_N}{(p^\mu)^2 - m_N^2}, & S_\Delta^{\mu\nu}(p) &= \frac{\not{p} + m_\Delta}{(p^\mu)^2 - m_\Delta^2} \left[-g^{\mu\nu} + \frac{1}{3}\gamma^\mu\gamma^\nu + \frac{2p^\mu p^\nu}{3m_\Delta^2} - \frac{p^\mu\gamma^\nu - p^\nu\gamma^\mu}{3m_\Delta} \right], \\ S_\rho(p) &= \frac{1}{(p^\mu)^2 - m_\rho^2}, & S_\sigma(p) &= \frac{1}{(p^\mu)^2 - m_{\sigma_0}^2}, \end{aligned} \quad (\text{C7})$$

where the physical masses m_N , m_Δ , m_ρ are used for the N , Δ , and ρ exchanges, while the bare mass m_{σ_0} is used for the σ exchange. The dipole form factor \mathcal{F} was defined in Eq. (36). I note that I use an idea of the unitary transformation method [56, 62] to calculate denominators of the propagators. Owing to the treatment of the energies of the four-momenta in Eq. (B2), these interaction terms are independent of the center-of-mass energy E .

2. $\pi N \rightarrow \eta N$

The $\pi^i N \rightarrow \eta N$ interactions, where the ηN state is purely isospin $I = 1/2$, are given as

$$V_{\pi N \rightarrow \eta N} = \bar{u}_N(-\mathbf{q}', \lambda_{N'}) (\bar{V}_{2a} + \bar{V}_{2b}) u_N(-\mathbf{q}, \lambda_N), \quad (\text{C8})$$

with

$$\bar{V}_{2a} = (\tau^i) \left[-\frac{(D+F)(D-3F)}{4\sqrt{3}f_\pi f_\eta} \right] \not{k}' \gamma_5 \frac{S_N(p+k) + S_N(p'+k')}{2} \not{k} \gamma_5 \mathcal{F}(\Lambda_{\eta NN}, q') \mathcal{F}(\Lambda_{\pi NN}, q), \quad (\text{C9})$$

$$\bar{V}_{2b} = (\tau^i) \left[-\frac{(D+F)(D-3F)}{4\sqrt{3}f_\pi f_\eta} \right] \not{k}' \gamma_5 \frac{S_N(p-k') + S_N(p'-k)}{2} \not{k} \gamma_5 \mathcal{F}(\Lambda_{\eta NN}, q') \mathcal{F}(\Lambda_{\pi NN}, q). \quad (\text{C10})$$

3. $\eta N \rightarrow \eta N$

The $\eta N \rightarrow \eta N$ interactions are given as

$$V_{\eta N \rightarrow \eta N} = \bar{u}_N(-\mathbf{q}', \lambda_{N'}) (\bar{V}_{3a} + \bar{V}_{3b}) u_N(-\mathbf{q}, \lambda_N), \quad (\text{C11})$$

with

$$\bar{V}_{3a} = \left(\frac{D-3F}{2\sqrt{3}f_\eta} \right)^2 \not{k}' \gamma_5 \frac{S_N(p+k) + S_N(p'+k')}{2} \not{k} \gamma_5 \mathcal{F}(\Lambda_{\eta NN}, q') \mathcal{F}(\Lambda_{\eta NN}, q), \quad (\text{C12})$$

$$\bar{V}_{3b} = \left(\frac{D-3F}{2\sqrt{3}f_\eta} \right)^2 \not{k}' \gamma_5 \frac{S_N(p-k') + S_N(p'-k)}{2} \not{k} \gamma_5 \mathcal{F}(\Lambda_{\eta NN}, q') \mathcal{F}(\Lambda_{\eta NN}, q). \quad (\text{C13})$$

4. $\pi N \rightarrow \sigma N$

The $\pi^i N \rightarrow \sigma N$ interactions, where the σN state is purely $I = 1/2$, are given as

$$V_{\pi N \rightarrow \sigma N} = \bar{u}_N(-\mathbf{q}', \lambda_{N'}) (\bar{V}_{4a} + \bar{V}_{4b} + \bar{V}_{4c}) u_N(-\mathbf{q}, \lambda_N), \quad (\text{C14})$$

with

$$\bar{V}_{4a} = (\tau^i) \frac{g_{\sigma NN}(D+F)}{2f_\pi} \frac{S_N(p+k) + S_N(p'+k')}{2} \not{k}' \gamma_5 \mathcal{F}(\Lambda_{\sigma NN}, q') \mathcal{F}(\Lambda_{\pi NN}, q), \quad (\text{C15})$$

$$\bar{V}_{4b} = (\tau^i) \frac{g_{\sigma NN}(D+F)}{2f_\pi} \not{k}' \gamma_5 \frac{S_N(p-k') + S_N(p'-k)}{2} \mathcal{F}(\Lambda_{\sigma NN}, q') \mathcal{F}(\Lambda_{\pi NN}, q), \quad (\text{C16})$$

$$\bar{V}_{4c} = (\tau^i) \left[-\frac{g_{\pi\pi\sigma}(D+F)}{2m_\pi f_\pi} \right] k_\mu (k-k')^\mu (\not{k} - \not{k}') \gamma_5 S_\pi(p'-p) \mathcal{F}(\Lambda_{\pi\pi\sigma}, |\mathbf{q} - \mathbf{q}'|) \mathcal{F}(\Lambda_{\pi NN}, |\mathbf{q} - \mathbf{q}'|). \quad (\text{C17})$$

The π propagator is

$$S_\pi(p) = \frac{1}{(p^\mu)^2 - m_\pi^2}, \quad (\text{C18})$$

with the physical pion mass m_π . I do not include the pion propagator of $S_\pi(k-k')$ for \bar{V}_{4c} because the $\pi\pi\sigma$ vertex interaction is “real” and hence it causes divergence. Similarly, I will omit propagators of momenta associated with the “real” vertex interactions.

5. $\eta N \rightarrow \sigma N$

The $\eta N \rightarrow \sigma N$ interactions are given as

$$V_{\eta N \rightarrow \sigma N} = \bar{u}_N(-\mathbf{q}', \lambda_{N'}) (\bar{V}_{5a} + \bar{V}_{5b}) u_N(-\mathbf{q}, \lambda_N), \quad (\text{C19})$$

with

$$\bar{V}_{5a} = -\frac{g_{\sigma NN}(D-3F)}{2\sqrt{3}f_\eta} \frac{S_N(p+k) + S_N(p'+k')}{2} \not{k}\gamma_5 \mathcal{F}(\Lambda_{\sigma NN}, q') \mathcal{F}(\Lambda_{\eta NN}, q), \quad (\text{C20})$$

$$\bar{V}_{5b} = -\frac{g_{\sigma NN}(D-3F)}{2\sqrt{3}f_\eta} \not{k}\gamma_5 \frac{S_N(p-k') + S_N(p'-k)}{2} \mathcal{F}(\Lambda_{\sigma NN}, q') \mathcal{F}(\Lambda_{\eta NN}, q). \quad (\text{C21})$$

6. $\sigma N \rightarrow \sigma N$

The $\sigma N \rightarrow \sigma N$ interactions are given as

$$V_{\sigma N \rightarrow \sigma N} = \bar{u}_N(-\mathbf{q}', \lambda_{N'}) (\bar{V}_{6a} + \bar{V}_{6b}) u_N(-\mathbf{q}, \lambda_N), \quad (\text{C22})$$

with

$$\bar{V}_{6a} = g_{\sigma NN}^2 \frac{S_N(p+k) + S_N(p'+k')}{2} \mathcal{F}(\Lambda_{\sigma NN}, q') \mathcal{F}(\Lambda_{\sigma NN}, q), \quad (\text{C23})$$

$$\bar{V}_{6b} = g_{\sigma NN}^2 \frac{S_N(p-k') + S_N(p'-k)}{2} \mathcal{F}(\Lambda_{\sigma NN}, q') \mathcal{F}(\Lambda_{\sigma NN}, q). \quad (\text{C24})$$

7. $\pi N \rightarrow \rho N$

The $\pi^i N \rightarrow \rho^j N$ interactions are given as

$$V_{\pi N \rightarrow \rho N} = e_{\rho\mu}^*(\mathbf{q}', \lambda_{M'}) \bar{u}_N(-\mathbf{q}', \lambda_{N'}) (\bar{V}_{7a}^\mu + \bar{V}_{7b}^\mu + \bar{V}_{7c}^\mu + \bar{V}_{7d}^\mu) u_N(-\mathbf{q}, \lambda_N), \quad (\text{C25})$$

with

$$\bar{V}_{7a}^\mu = (\tau^j \tau^i) \frac{g_{\rho NN}(D+F)}{4f_\pi} \left[\gamma^\mu + \frac{\kappa_\rho}{4m_N} (\gamma^\mu \not{k}' - \not{k}' \gamma^\mu) \right] \frac{S_N(p+k) + S_N(p'+k')}{2} \not{k}\gamma_5 \mathcal{F}(\Lambda_{\rho NN}, q') \mathcal{F}(\Lambda_{\pi NN}, q), \quad (\text{C26})$$

$$\bar{V}_{7b}^\mu = (\tau^i \tau^j) \frac{g_{\rho NN}(D+F)}{4f_\pi} \not{k}\gamma_5 \frac{S_N(p-k') + S_N(p'-k)}{2} \left[\gamma^\mu + \frac{\kappa_\rho}{4m_N} (\gamma^\mu \not{k}' - \not{k}' \gamma^\mu) \right] \mathcal{F}(\Lambda_{\rho NN}, q') \mathcal{F}(\Lambda_{\pi NN}, q), \quad (\text{C27})$$

$$\bar{V}_{7c}^\mu = (i\epsilon_{jik} \tau^k) \frac{g_{\pi\rho\rho}(D+F)}{2f_\pi} (2k^\mu - k'^\mu) (\not{k} - \not{k}') \gamma_5 S_\pi(p'-p) \mathcal{F}(\Lambda_{\pi\rho\rho}, |\mathbf{q} - \mathbf{q}'|) \mathcal{F}(\Lambda_{\pi NN}, |\mathbf{q} - \mathbf{q}'|), \quad (\text{C28})$$

$$\bar{V}_{7d}^\mu = (i\epsilon_{jik} \tau^k) \left[-\frac{g_{\rho NN}(D+F)}{2f_\pi} \right] \gamma^\mu \gamma_5 \mathcal{F}(\Lambda_{\rho NN}, q') \mathcal{F}(\Lambda_{\pi NN}, q). \quad (\text{C29})$$

8. $\eta N \rightarrow \rho N$

The $\eta N \rightarrow \rho^j N$ interactions are given as

$$V_{\eta N \rightarrow \rho N} = e_{\rho\mu}^*(\mathbf{q}', \lambda_{M'}) \bar{u}_N(-\mathbf{q}', \lambda_{N'}) (\bar{V}_{8a}^\mu + \bar{V}_{8b}^\mu) u_N(-\mathbf{q}, \lambda_N), \quad (\text{C30})$$

with

$$\bar{V}_{8a}^\mu = (\tau^j) \left[-\frac{g_{\rho NN}(D-3F)}{4\sqrt{3}f_\eta} \right] \left[\gamma^\mu + \frac{\kappa_\rho}{4m_N} (\gamma^\mu \not{k}' - \not{k}' \gamma^\mu) \right] \frac{S_N(p+k) + S_N(p'+k')}{2} \not{k}\gamma_5 \mathcal{F}(\Lambda_{\rho NN}, q') \mathcal{F}(\Lambda_{\eta NN}, q), \quad (\text{C31})$$

$$\bar{V}_{8b}^\mu = (\tau^j) \left[-\frac{g_{\rho NN}(D-3F)}{4\sqrt{3}f_\eta} \right] \not{k}\gamma_5 \frac{S_N(p-k') + S_N(p'-k)}{2} \left[\gamma^\mu + \frac{\kappa_\rho}{4m_N} (\gamma^\mu \not{k}' - \not{k}' \gamma^\mu) \right] \mathcal{F}(\Lambda_{\rho NN}, q') \mathcal{F}(\Lambda_{\eta NN}, q). \quad (\text{C32})$$

9. $\sigma N \rightarrow \rho N$

The $\sigma N \rightarrow \rho^j N$ interactions are given as

$$V_{\sigma N \rightarrow \rho N} = e_{\rho\mu}^*(\mathbf{q}', \lambda_{M'}) \bar{u}_N(-\mathbf{q}', \lambda_{N'}) (\bar{V}_{9a}^\mu + \bar{V}_{9b}^\mu) u_N(-\mathbf{q}, \lambda_N), \quad (\text{C33})$$

with

$$\bar{V}_{9a}^\mu = (\tau^j) \frac{g_{\rho NN} g_{\sigma NN}}{2} \left[\gamma^\mu + \frac{\kappa_\rho}{4m_N} (\gamma^\mu \not{k}' - \not{k}' \gamma^\mu) \right] \frac{S_N(p+k) + S_N(p'+k')}{2} \mathcal{F}(\Lambda_{\rho NN}, q') \mathcal{F}(\Lambda_{\sigma NN}, q), \quad (\text{C34})$$

$$\bar{V}_{9b}^\mu = (\tau^j) \frac{g_{\rho NN} g_{\sigma NN}}{2} \frac{S_N(p-k') + S_N(p'-k)}{2} \left[\gamma^\mu + \frac{\kappa_\rho}{4m_N} (\gamma^\mu \not{k}' - \not{k}' \gamma^\mu) \right] \mathcal{F}(\Lambda_{\rho NN}, q') \mathcal{F}(\Lambda_{\sigma NN}, q). \quad (\text{C35})$$

10. $\rho N \rightarrow \rho N$

The $\rho^i N \rightarrow \rho^j N$ interactions are given as

$$V_{\rho N \rightarrow \rho N} = e_{\rho\mu}^*(\mathbf{q}', \lambda_{M'}) \bar{u}_N(-\mathbf{q}', \lambda_{N'}) (\bar{V}_{10a}^{\mu\nu} + \bar{V}_{10b}^{\mu\nu} + \bar{V}_{10c}^{\mu\nu}) e_{\rho\nu}(\mathbf{q}, \lambda_M) u_N(-\mathbf{q}, \lambda_N), \quad (\text{C36})$$

with

$$\begin{aligned} \bar{V}_{10a}^{\mu\nu} = & (\tau^j \tau^i) \frac{g_{\rho NN}^2}{4} \left[\gamma^\mu + \frac{\kappa_\rho}{4m_N} (\gamma^\mu \not{k}' - \not{k}' \gamma^\mu) \right] \frac{S_N(p+k) + S_N(p'+k')}{2} \left[\gamma^\nu - \frac{\kappa_\rho}{4m_N} (\gamma^\nu \not{k} - \not{k} \gamma^\nu) \right] \\ & \times \mathcal{F}(\Lambda_{\rho NN}, q') \mathcal{F}(\Lambda_{\rho NN}, q), \end{aligned} \quad (\text{C37})$$

$$\begin{aligned} \bar{V}_{10b}^{\mu\nu} = & (\tau^i \tau^j) \frac{g_{\rho NN}^2}{4} \left[\gamma^\nu - \frac{\kappa_\rho}{4m_N} (\gamma^\nu \not{k} - \not{k} \gamma^\nu) \right] \frac{S_N(p-k') + S_N(p'-k)}{2} \left[\gamma^\mu + \frac{\kappa_\rho}{4m_N} (\gamma^\mu \not{k}' - \not{k}' \gamma^\mu) \right] \\ & \times \mathcal{F}(\Lambda_{\rho NN}, q') \mathcal{F}(\Lambda_{\rho NN}, q), \end{aligned} \quad (\text{C38})$$

$$\bar{V}_{10c}^{\mu\nu} = (i\epsilon_{jik} \tau^k) \frac{g_{\rho NN}^2 \kappa_\rho}{8m_N} (\gamma^\nu \gamma^\mu - \gamma^\mu \gamma^\nu) \mathcal{F}(\Lambda_{\rho NN}, q') \mathcal{F}(\Lambda_{\rho NN}, q). \quad (\text{C39})$$

11. $\pi N \rightarrow \pi \Delta$

The $\pi^i N \rightarrow \pi^j \Delta$ interaction is given as

$$V_{\pi N \rightarrow \pi \Delta} = \bar{u}_{\Delta\mu}(-\mathbf{q}', \lambda_{\Delta'}) (\bar{V}_{11a}^\mu + \bar{V}_{11b}^\mu) u_N(-\mathbf{q}, \lambda_N), \quad (\text{C40})$$

with

$$\bar{V}_{11a}^\mu = (T^{\dagger j} \tau^i) \frac{f_{\pi N \Delta} (D+F)}{2m_\pi f_\pi} k'^\mu \frac{S_N(p+k) + S_N(p'+k')}{2} \not{k} \gamma_5 \mathcal{F}(\Lambda_{\pi N \Delta}, q') \mathcal{F}(\Lambda_{\pi NN}, q), \quad (\text{C41})$$

$$\bar{V}_{11b}^\mu = (T^{\dagger i} \tau^j) \frac{f_{\pi N \Delta} (D+F)}{2m_\pi f_\pi} k^\mu S_N(p-k') \not{k}' \gamma_5 \mathcal{F}(\Lambda_{\pi NN}, q') \mathcal{F}(\Lambda_{\pi N \Delta}, q). \quad (\text{C42})$$

12. $\eta N \rightarrow \pi \Delta$

The $\eta N \rightarrow \pi^j \Delta$ interaction is given as

$$V_{\eta N \rightarrow \pi \Delta} = \bar{u}_{\Delta\mu}(-\mathbf{q}', \lambda_{\Delta'}) \bar{V}_{12}^\mu u_N(-\mathbf{q}, \lambda_N), \quad (\text{C43})$$

with

$$\bar{V}_{12}^\mu = (T^{\dagger j}) \left[-\frac{f_{\pi N \Delta} (D-3F)}{2\sqrt{3}m_\pi f_\eta} \right] k'^\mu \frac{S_N(p+k) + S_N(p'+k')}{2} \not{k} \gamma_5 \mathcal{F}(\Lambda_{\pi N \Delta}, q') \mathcal{F}(\Lambda_{\eta NN}, q). \quad (\text{C44})$$

13. $\sigma N \rightarrow \pi \Delta$

The $\sigma N \rightarrow \pi^j \Delta$ interaction is given as

$$V_{\sigma N \rightarrow \pi \Delta} = \bar{u}_{\Delta\mu}(-\mathbf{q}', \lambda_{\Delta'}) \bar{V}_{13}^{\mu} u_N(-\mathbf{q}, \lambda_N), \quad (\text{C45})$$

with

$$\bar{V}_{13}^{\mu} = (T^{\dagger j}) \frac{g_{\sigma NN} f_{\pi N \Delta}}{m_{\pi}} k'^{\mu} \frac{S_N(p+k) + S_N(p'+k')}{2} \mathcal{F}(\Lambda_{\pi N \Delta}, q') \mathcal{F}(\Lambda_{\sigma NN}, q). \quad (\text{C46})$$

14. $\rho N \rightarrow \pi \Delta$

The $\rho^i N \rightarrow \pi^j \Delta$ interaction is given as

$$V_{\rho N \rightarrow \pi \Delta} = \bar{u}_{\Delta\mu}(-\mathbf{q}', \lambda_{\Delta'}) \bar{V}_{14}^{\mu\nu} e_{\rho\nu}(\mathbf{q}, \lambda_M) u_N(-\mathbf{q}, \lambda_N), \quad (\text{C47})$$

with

$$\bar{V}_{14}^{\mu\nu} = (T^{\dagger j} \tau^i) \frac{g_{\rho NN} f_{\pi N \Delta}}{2m_{\pi}} k'^{\mu} \frac{S_N(p+k) + S_N(p'+k')}{2} \left[\gamma^{\nu} - \frac{\kappa_{\rho}}{4m_N} (\gamma^{\nu} \not{k} - \not{k} \gamma^{\nu}) \right] \mathcal{F}(\Lambda_{\pi N \Delta}, q') \mathcal{F}(\Lambda_{\rho NN}, q). \quad (\text{C48})$$

15. $\pi \Delta \rightarrow \pi \Delta$

The $\pi^i \Delta \rightarrow \pi^j \Delta$ interaction is given as

$$V_{\pi \Delta \rightarrow \pi \Delta} = \bar{u}_{\Delta\mu}(-\mathbf{q}', \lambda_{\Delta'}) \bar{V}_{15}^{\mu\nu} u_{\Delta\nu}(-\mathbf{q}, \lambda_{\Delta}), \quad (\text{C49})$$

with

$$\bar{V}_{15}^{\mu\nu} = (T^{\dagger j} T^i) \left(\frac{f_{\pi N \Delta}}{m_{\pi}} \right)^2 k'^{\mu} \frac{S_N(p+k) + S_N(p'+k')}{2} k^{\nu} \mathcal{F}(\Lambda_{\pi N \Delta}, q') \mathcal{F}(\Lambda_{\pi N \Delta}, q). \quad (\text{C50})$$

16. s -channel exchange of bare N^* and Δ^* states

To take into account the bare N^* and Δ^* states for the meson–baryon scattering in s channel, I add

$$V_{jk}^{\text{bare}}(E; q', q) = \frac{g_j g_k}{2m_{\pi}(E - M_0)} \left(\frac{q'}{m_{\pi}} \right)^{L'} \left(\frac{q}{m_{\pi}} \right)^L \mathcal{F}(\Lambda, q') \mathcal{F}(\Lambda, q), \quad (\text{C51})$$

to the corresponding partial-wave components $V_{\alpha, jk}$ in Eq. (1). Here, M_0 is the bare mass of the N^* and Δ^* states, g_j is the coupling constant for the bare state to the j th meson–baryon channel, and Λ is the cutoff. I note that only this bare-state contribution depends on the center-of-mass energy E among the meson–baryon interaction terms.

-
- [1] P. A. Zyla *et al.* [Particle Data Group], PTEP **2020**, 083C01 (2020).
[2] M. Y. Han and Y. Nambu, Phys. Rev. **139**, B1006 (1965).
[3] O. Krehl, C. Hanhart, S. Krewald and J. Speth, Phys. Rev. C **62**, 025207 (2000).
[4] G. Y. Chen, S. S. Kamalov, S. N. Yang, D. Drechsel and L. Tiator, Phys. Rev. C **76**, 035206 (2007).
[5] D. Rönchen, M. Döring, F. Huang, H. Haberzettl,

- J. Haidenbauer, C. Hanhart, S. Krewald, U. G. Meißner and K. Nakayama, Eur. Phys. J. A **49**, 44 (2013).
[6] H. Kamano, S. X. Nakamura, T. S. H. Lee and T. Sato, Phys. Rev. C **88**, 035209 (2013).
[7] A. V. Anisovich, R. Beck, E. Klempt, V. A. Nikonov, A. V. Sarantsev and U. Thoma, Eur. Phys. J. A **48**, 15 (2012).
[8] R. L. Workman, R. A. Arndt, W. J. Briscoe, M. W. Paris

- and I. I. Strakovsky, Phys. Rev. C **86**, 035202 (2012).
- [9] C. B. Lang, L. Leskovec, M. Padmanath and S. Prelovsek, Phys. Rev. D **95**, 014510 (2017).
- [10] Z. W. Liu, W. Kamleh, D. B. Leinweber, F. M. Stokes, A. W. Thomas and J. J. Wu, Phys. Rev. Lett. **116**, 082004 (2016).
- [11] Z. W. Liu, W. Kamleh, D. B. Leinweber, F. M. Stokes, A. W. Thomas and J. J. Wu, Phys. Rev. D **95**, 034034 (2017).
- [12] J. J. Wu, H. Kamano, T. S. H. Lee, D. B. Leinweber and A. W. Thomas, Phys. Rev. D **95**, 114507 (2017).
- [13] J. J. Wu, D. B. Leinweber, Z. W. Liu and A. W. Thomas, Phys. Rev. D **97**, 094509 (2018).
- [14] J. Segovia, B. El-Bennich, E. Rojas, I. C. Cloet, C. D. Roberts, S. S. Xu and H. S. Zong, Phys. Rev. Lett. **115**, 171801 (2015).
- [15] D. Rönchen, M. Döring, F. Huang, H. Haberzettl, J. Haidenbauer, C. Hanhart, S. Krewald, U. G. Meißner and K. Nakayama, Eur. Phys. J. A **50**, 101 (2014) [erratum: Eur. Phys. J. A **51**, 63 (2015)].
- [16] T. Mart, S. Clymton and A. J. Arifi, Phys. Rev. D **92**, 094019 (2015).
- [17] D. Rönchen, M. Döring, H. Haberzettl, J. Haidenbauer, U. G. Meißner and K. Nakayama, Eur. Phys. J. A **51**, 70 (2015).
- [18] A. V. Anisovich, R. Beck, M. Döring, M. Gottschall, J. Hartmann, V. Kashevarov, E. Klempt, U. G. Meißner, V. Nikonov and M. Ostrick, *et al.* Eur. Phys. J. A **52**, 284 (2016).
- [19] H. Kamano, S. X. Nakamura, T. S. H. Lee and T. Sato, Phys. Rev. C **94**, 015201 (2016).
- [20] C. Chen, B. El-Bennich, C. D. Roberts, S. M. Schmidt, J. Segovia and S. Wan, Phys. Rev. D **97**, 034016 (2018).
- [21] D. Rönchen, M. Döring and U. G. Meißner, Eur. Phys. J. A **54**, 110 (2018).
- [22] C. Chen, G. I. Krein, C. D. Roberts, S. M. Schmidt and J. Segovia, Phys. Rev. D **100**, 054009 (2019).
- [23] T. Sekihara, Phys. Rev. C **95**, 025206 (2017).
- [24] T. Hyodo, D. Jido and A. Hosaka, Phys. Rev. C **85**, 015201 (2012).
- [25] F. Aceti and E. Oset, Phys. Rev. D **86**, 014012 (2012).
- [26] T. Hyodo, Int. J. Mod. Phys. A **28**, 1330045 (2013).
- [27] T. Sekihara, T. Hyodo and D. Jido, PTEP **2015**, 063D04 (2015).
- [28] F. Aceti, L. R. Dai, L. S. Geng, E. Oset and Y. Zhang, Eur. Phys. J. A **50**, 57 (2014).
- [29] H. Nagahiro and A. Hosaka, Phys. Rev. C **90**, 065201 (2014).
- [30] Y. Kamiya and T. Hyodo, Phys. Rev. C **93**, 035203 (2016).
- [31] T. Sekihara, T. Arai, J. Yamagata-Sekihara and S. Yasui, Phys. Rev. C **93**, 035204 (2016).
- [32] Z. H. Guo and J. A. Oller, Phys. Rev. D **93**, 054014 (2016).
- [33] Z. H. Guo and J. A. Oller, Phys. Rev. D **93**, 096001 (2016).
- [34] J. X. Lu, H. X. Chen, Z. H. Guo, J. Nieves, J. J. Xie and L. S. Geng, Phys. Rev. D **93**, 114028 (2016).
- [35] X. W. Kang, Z. H. Guo and J. A. Oller, Phys. Rev. D **94**, 014012 (2016).
- [36] M. Albaladejo, D. Jido, J. Nieves and E. Oset, Eur. Phys. J. C **76**, 300 (2016).
- [37] Y. Kamiya and T. Hyodo, PTEP **2017**, 023D02 (2017).
- [38] Y. Kamiya and T. Hyodo, Phys. Rev. D **97**, 054019 (2018).
- [39] Y. Tsuchida and T. Hyodo, Phys. Rev. C **97**, 055213 (2018).
- [40] J. A. Oller, Annals Phys. **396**, 429-458 (2018).
- [41] Z. H. Guo and J. A. Oller, Phys. Lett. B **793**, 144-149 (2019).
- [42] F. K. Guo, C. Hanhart, U. G. Meißner, Q. Wang, Q. Zhao and B. S. Zou, Rev. Mod. Phys. **90**, 015004 (2018).
- [43] J. A. Oller, Prog. Part. Nucl. Phys. **110**, 103728 (2020).
- [44] S. Weinberg, Phys. Rev. **137**, B672-B678 (1965).
- [45] E. Hernandez and A. Mondragon, Phys. Rev. C **29**, 722-738 (1984).
- [46] S. Aoyama, T. Myo, K. Kato and K. Ikeda, Prog. Theor. Phys. **116**, 1 (2006).
- [47] T. Myo and K. Kato, PTEP **2020**, 12A101 (2020).
- [48] INS Data Analysis Center, the George Washington University: <http://gwdac.phys.gwu.edu> (date last accessed March 18, 2021).
- [49] B. Julia-Diaz, T. S. H. Lee, A. Matsuyama and T. Sato, Phys. Rev. C **76**, 065201 (2007).
- [50] H. Kamano, B. Julia-Diaz, T. S. H. Lee, A. Matsuyama and T. Sato, Phys. Rev. C **79**, 025206 (2009).
- [51] A. Matsuyama, T. Sato and T. S. H. Lee, Phys. Rept. **439**, 193-253 (2007).
- [52] V. D. Burkert and C. D. Roberts, Rev. Mod. Phys. **91**, 011003 (2019).
- [53] N. Suzuki, B. Julia-Diaz, H. Kamano, T. S. H. Lee, A. Matsuyama and T. Sato, Phys. Rev. Lett. **104**, 042302 (2010).
- [54] B. Golli, H. Osmanović, S. Širca and A. Švarc, Phys. Rev. C **97**, 035204 (2018).
- [55] G. F. Chew and F. E. Low, Phys. Rev. **101**, 1570-1579 (1956).
- [56] T. Sato and T. S. H. Lee, J. Phys. G **36**, 073001 (2009).
- [57] B. Golli, H. Osmanović and S. Širca, Phys. Rev. C **100**, 035204 (2019).
- [58] H. Kamano, S. X. Nakamura, T. S. H. Lee and T. Sato, Phys. Rev. C **90**, 065204 (2014).
- [59] H. Kamano, S. X. Nakamura, T. S. H. Lee and T. Sato, Phys. Rev. C **92**, 025205 (2015) [erratum: Phys. Rev. C **95**, 049903 (2017)].
- [60] M. Jacob and G. C. Wick, Annals Phys. **7**, 404-428 (1959).
- [61] T. Sekihara, Y. Kamiya and T. Hyodo, Phys. Rev. C **98**, 015205 (2018).
- [62] T. Sato and T. S. H. Lee, Phys. Rev. C **54**, 2660-2684 (1996).